https://doi.org/10.5194/egusphere-2024-371
Preprint. Discussion started: 23 February 2024

A modelled multi-decadal hailday time series for Switzerland

Lena Wilhelm[1], Cornelia Schwierz[2], Katharina Schröer[3], Mateusz Taszarek[4], and Olivia Martius[1]

[1]Institute of Geography, Oeschger Centre for Climate Change Research, University of Bern, Bern, Switzerland
[2]Office of Meteorology and Climatology, MeteoSwiss, Zurich, Switzerland
[3]Institute of Environmental Social Sciences and Geography, University of Freiburg, Freiburg, Germany
[4]Department of Meteorology and Climatology, Adam Mickiewicz University, Poznan, Poland

Correspondence: Lena Wilhelm (lena.wilhelm@unibe.ch)

Abstract. In Switzerland, hail is one of the costliest natural hazards, causing extensive damage to agriculture, cars, and infrastructure each year. In a warming climate, hail frequency and its patterns of occurrence are expected to change, which is why understanding the long-term variability and its drivers is essential. Therefore, this study presents new multidecadal daily hail time series for Northern and Southern Switzerland from 1959 to 2022. Daily radar hail proxies and environmental predictor variables from ERA-5 reanalysis are used to build an ensemble statistical model for predicting past hail occurrence. Haildays are identified from operational radar-derived "Probability of Hail" (POH) data for two study regions, namely the north and south of the Swiss Alps. We use data from 2002 - 2022 during the convective season from April to September. The decision hailday YES / NO is based on surpassing a POH $\geq 80\%$ for a certain minimum footprint area of the domains. Separate logistic regression models and GAM´s are built for each domain and combined in an ensemble model to reconstruct the final time series. Overall, the models are able to describe the observed time series well. Historical hail reports are used for comparing years with the most and least haildays. For the northern and southern domains, the time series both show a significant positive trend in yearly aggregated haildays from 1959 to 2022. The trend is still positive and significant when looking at the period 1979–2022. In all models, the trends are driven by moisture and instability predictors. In the last two decades, we can see an increase in haildays at the beginning of the hail season and an earlier and longer peak, however, there is no systematic shift in the seasonal cycle. With this time series, we can now study the local and remote drivers of the interannual variability and seasonality of Swiss hail occurrence.

1 Introduction

During the convective season, hail causes substantial damage to agriculture, cars, and buildings in Switzerland (BAFU, 2012). One extreme hailstorm on 21 June 2021 caused building damages of 400 million Swiss francs (CHF, approx. 415 million EUR) in a single canton alone (Schmid et al., 2023; Kopp et al., 2023). Addressing hail hazard is difficult, as hail is related to severe thunderstorms, one of the most complicated meteorological phenomena. Thunderstorms feature a small spatial scale, vigorous development, and intricate physical interactions ranging from synoptic to microphysical spatial dimensions. Predicting the development and evolution of convective storms is especially challenging in the complex topography of Western Europe. Orography, such as the Alps and Jura Mountains, can initiate or modulate convection, for example by enhancing environmental

https://doi.org/10.5194/egusphere-2024-371
Preprint. Discussion started: 23 February 2024

wind shear that can lead to better storm organization (Kaltenboeck and Steinheimer, 2015; Kunz et al., 2018). In a changing climate, we may also expect changes in hail frequency and intensity. While there are indications of increasing hail frequency and size (e.g. Raupach et al. (2023a); Battaglioli et al. (2023a); Púčik et al. (2019)) and hail damage (e.g. Willemse (1995), SwissRe (from personal communication)) in Europe, there are also studies showing a negative or no trend (e.g. Augenstein et al. (2023)). It is important to mention that trends in damages are not necessarily driven by trends in the hazard. Damages are linked to exposure and vulnerability and undergo changes with urban expansion and changes in the infrastructure.

With hail frequency hotspots in the Jura, the Entlebuch, and in southern Switzerland, the pre-Alpine regions north and south of the Alps are affected most often by hailstorms in Switzerland (Nisi et al., 2016). Hail occurrence has a strong year-to-year variability (Schröer et al., 2023). Recent studies (Barras et al., 2021; Nisi et al., 2018, 2020; Schröer et al., 2023) revealed that there is a large difference in interannual hail variability between the north and the south side of the Alps. Understanding the drivers of the interannual variability and changes in seasonality is essential for potential adaptation strategies, e.g. regarding agricultural hail losses. In contrast to North America, where important drivers of the year-to-year variability of severe convection and hail are well studied (Tippett et al., 2015; Allen et al., 2020; Taszarek et al., 2020a; Nixon et al., 2023), a thorough examination of the long-term variability of hail in Switzerland is currently missing. Unfortunately, the lack of long-term direct hail observations often hinders the analysis of hail patterns and variability (Martius et al., 2015). To be able to analyse long-term trends and variability in hail occurrence, we require hail time series that are longer than the currently available observations. Environmental hail proxies derived from sounding, re-analysis, or model data in combination with statistical models are typically used to create such extended time series. The primary advantage of reanalysis data is their spatial and temporal coverage, as well as their availability across longer time periods. Therefore, this study uses ERA-5 data to produce a multidecadal hailday time series for Northern and Southern Switzerland from 1959 to 2022. Recent studies have shown that ERA-5 can be considered as one of the most reliable reanalysis in representing convective storm environments (Li et al., 2020; Taszarek et al., 2020b; Pilguj et al., 2022; Varga and Breuer, 2022; Wu et al., 2024).

A combination of multiple mesoscale variables is required to estimate the hail potential of the atmosphere. The development of a hailstorm requires an unstable atmosphere, high lower tropospheric moisture, a sufficient vertical wind shear and a lifting mechanism (e.g. Johns and Doswell (1992); Battaglioli et al. (2023a); Johnson and Sugden (2021); Kumjian and Lombardo (2020); Kumjian et al. (2021). Several studies have shown that both mesoscale and synoptic flow-conditions, including the presence of fronts, and their interaction with complex terrain are significant factors driving hail formation in Europe (e.g. Brooks et al. (2003, 2007); Cacciamani et al. (1995); Costa et al. (2001); Giaiotti et al. (2003); Kunz and Puskeiler (2010); Piasecki et al. (2023)). Regional characteristics, such as terrain barriers, local wind systems, or warm water surfaces influence the relative importance of the four components necessary for hail formation, which is why this study looks at the region north and south of the Alps separately. The region north of the Alps is exposed to frontal systems arising from the west (or north), as there is no barrier by a high mountain range like in the southern region (Schemm et al., 2016). The region south of the Alps is influenced by the advection of moist and warm air masses from the southwest or south and is protected from northern air masses by the Alpine chain (Schemm et al., 2016). In addition, Cacciamani et al. (1995) showed, that in the Po valley,

https://doi.org/10.5194/egusphere-2024-371
Preprint. Discussion started: 23 February 2024

hailstorm formation is almost always associated with some synoptic-scale dynamical forcing and not only depends on pure local thermodynamic conditions.

Various mesoscale variables have been used in statistical models to predict severe (hail producing) thunderstorms in Europe (e.g. Groenemeijer and van Delden (2007); Kunz (2007); García-Ortega et al. (2012); Manzato (2012); Mohr and Kunz (2013); Gascón et al. (2015); Púčik et al. (2015); Tuovinen et al. (2015); Melcón et al. (2017)). Note that there are regional differences to the U. S. (e.g. Brooks et al. (2003); Rasmussen (2003); Johnson and Sugden (2021); Taszarek et al. (2020a); Nixon et al. (2023)) and Australia (e.g. Allen et al. (2011); Raupach et al. (2023a)). Mohr and Kunz (2013) and Kunz (2007) presented a comprehensive list of hail-relevant meteorological parameters and indices that can be utilized as environmental proxies for Europe and Huntrieser et al. (1997) presented a list specifically for Switzerland. The variables can be grouped into the categories of instability, moisture (thermodynamic) and kinematic conditions. Latent, conditional and potential instabilities are captured by indices like the Vertical Total (Miller, 1972), Boyden Index (Boyden, 1963), Lifted Index (Galway, 1956), Showalter Index (Showalter, 1953), CAPE (Moncrieff and Miller, 1976), or the KO Index Andersson et al. (1989). There are also indices that combine all three instabilities, like the Total Totals (Miller, 1972) or the K Index (George, 1961). Other indices measure the tropospheric moisture content (e.g., vertically integrated liquid water; (Greene and Clark, 1972)), or kinematic conditions like the magnitude of vertical wind shear (Weisman and Klemp, 1982, 1984). Composite parameters like the SWISS Index (Huntrieser et al., 1997), Significant Hail Parameter (SHIP) or Hail Size Index (HSI) that combine kinematic and thermodynamic variables, also correlate well with the occurrence of large hail (Allen et al., 2015; Czernecki et al., 2019; Gensini et al., 2021; Johnson and Sugden, 2021). Such indices are then used in statistical models to estimate the occurrence of hail. For instance, Mohr et al. (2015a) used a logistic regression approach to estimate the potential for hailstorms in Germany between 1971 - 2000 and 2021 - 2050. They found, that the potential for hail events will increase in the future (2021–2050) compared to the past (1971–2000), but only statistically significant in the northwest and south of Germany. Logistic regression was also used by Billet et al. (1997); Sánchez et al. (2009); Schmeits et al. (2005) and López et al. (2007) to model thunderstorm or hail events. Recently Battaglioli et al. (2023a) created a logistic generalized additive model for Europe and the United States from ESWD reports and ERA-5 data to model trends of large hail (> 2cm and > 5cm) occurrence. They presented a strong significant increase in hail frequency in Northern Italy and parts of Southern Switzerland. Allen et al. (2015) used a Poisson regression model based on monthly averages to connect monthly hail frequency to the large-scale atmospheric environment in the United States. Madonna et al. (2018) presented a poisson regression hail model specifically for Northern Switzerland, using radar and ERA-5 data. Their model captured the intra- and inter-annual hail variability well and their time series showed an increase of 0.5 days per month per decade. This paper builds on the work of Madonna et al. (2018), however, here we increase the resolution of the analysis to daily, additionally include the South of Switzerland, and extend the time series back to 1959. As opposed to Battaglioli et al. (2023a) who used ESWD severe weather reports, we use radar data to model daily hail occurrence of any size at the ground, and we use an ensemble of two statistical models (logistic multiple regression and logistic generalized additive model (GAM)) leveraging the best-fitting predictors for each region individually. We include smaller sizes as we work with the POH radar product, which is a proxy for hail of any size at the ground. Additionally, even small hail can be damaging to agricultural produce (Katz and Garcia, 1981). We need to stress, that our goal is not to build a model usable

https://doi.org/10.5194/egusphere-2024-371
Preprint. Discussion started: 23 February 2024

for forecasting or that can be applied to other regions. We want to produce the best possible reconstruction of past haildays in Switzerland with the optimal combination of environmental predictor variables for the specific domains. The modelled time series will then be used to study long-term trends and changes in frequency, seasonality, and the variability of model-derived Swiss hailstorms in the past decades.

The paper is structured as follows. Section 2 gives an overview of the datasets used in this study, followed by a description of methods in Sect. 3. Model building and performance are explained in Sect. 4. Results from time series analyses are presented in Sect. 5, which are discussed in Sect. 6. Conclusions follow in Sect. 7.

2 Data

2.1 Radar-derived Probability of Hail

This study uses the radar- and model-based product POH (probability of hail) as a proxy for hail. POH is an empirical hail detection algorithm used operationally at MeteoSwiss that outputs the probability of hail of any size at the ground from 0 to 100%. The estimate follows the method from Foote et al. (2005) and Waldvogel et al. (1979) and is based on the vertical distance between the 45 dBz EchoTop height measured by the Swiss radar network and the freezing level height obtained from the numerical weather forecast model COSMO-CH ((Baldauf et al. (2011)), see Nisi et al. (2016) for a detailed description of the POH algorithm). POH is currently available from 2002 to 2023 in 5 min and daily temporal resolution on a 1 km x 1 km Cartesian grid. The 3rd generation Swiss radar network, which from 2002 to 2012 consisted of three single-polarization Doppler C-band radars, was updated to the more advanced 4th generation dual polarization Doppler C-band radars in 2012. In the following years, two additional radars were installed in mountainous regions at high elevations, where orographic beam shielding hindered the low-level visibility of the other three radars. We here use thoroughly quality-checked and reprocessed POH data of the recently published Swiss hail climatology (Trefalt et al., 2023; Schröer et al., 2023) and consider the area up to 140 km around the five radar stations (see Fig. 1) to minimize planar artifacts and ground clutter. The Central Alps are excluded from the analysis, as hail rarely occurs there and radar quality may be lower (Feldmann et al., 2021). The study regions correspond to the ones used in Barras et al. (2021). Nisi et al. (2016) showed that a threshold of POH $\geq 80\%$ best represents hail locally, comparing POH data with car insurance loss data. More information on the definition of haildays is described in Sect. 3.1.

2.1.1 ERA-5 environmental predictors

For multi-decadal analyses, at the moment, ERA-5 is the best available product for Europe. This is why we take environmental information to quantify the hail potential of the atmosphere from ERA–5 reanalysis data (Hersbach et al., 2020). In this work, data on model levels (137 levels from 1000 hPa to 1 hPa, 0.5° x 0.5° grid resolution), pressure levels (17 levels, 0.5° x 0.5 ° grid), and surface data (0.25° x 0.25 ° grid) in hourly and 6-hourly resolution was used from 1959 to 2022. We exclude any data before 1959 for our analysis, as the quality of ERA-5 declines in those years and should not be used to analyze trends

https://doi.org/10.5194/egusphere-2024-371
Preprint. Discussion started: 23 February 2024

or past changes. A total of 75 convective parameters was calculated (see Table A2), some of them with the help of MetPy. In models classifying hail, one would usually select the ERA-5 grid point proximal in time and space to the hail incident. For a reconstruction of past haildays that is not possible, as there is no information on the hail event before the start of the observational period. Our aim was also not to reconstruct every hail event perfectly for each pixel and timestep, but rather to reconstruct the occurrence of a hailday vs non-hailday. The way we define haildays focuses on days with more than just a single hail cell. The thresholds are such that they capture events that in the past lead to damages and that affect somewhat larger areas (POH $\geq 80\%$ over min. 580 (north) / 499 (south) km^2 of the domain, see Sect, 3.1). Hence, to model the occurrence of a hailday, we needed only one absolute value per day and per region of all convective parameters, that can then be related to the binary hailday time series from the POH data (see Sect. 3.1). The choice of which time and summary statistic was calculated for each variable draws on and extends extensive analyses by Trefalt (2017), who analyzed distributions of convection-related atmospheric variables on hail vs. non-haildays in Switzerland. For all variables used in the final models, the spatially averaged value at 12:00 UTC was chosen. The fact that the value at 12:00 shows good skill may be related to most storms in Switzerland occurring in the afternoon. Hence, this value may well capture the atmospheric condition inductive to storm formation. Instead of the mean at 12:00 UTC, we also tried many other options, such as choosing all convective parameters at the time and location of maximum CAPE, or other extremal statistics, but this did not improve model performance. This together with the fact that the resolution of ERA-5 does not capture all the relevant small-scale processes in Switzerland, lead us to choosing area mean values for modelling haildays. This suggests that the mean values contain sufficient information for a "simple" hail vs. no hail decision as opposed to determining more detailed parameters such as hail size. This may be due to less noise in the aggregated values. Trefalt (2017) also found, that for many convective parameters the separation of mean distributions of hail vs no hail was strong enough for differentiating between hail and non-hail days and did not always improve when comparing percentile or maxima / minima distributions.

2.2 Historic hail data

For plausibility checks we compared the modelled time series to a historical hail data set, which is a qualitative combination of multiple data sources, mainly damage reports ("historical"), reaching back to 1825 and early radar data ("modern"), including research radar data reaching back to 1983 (Meteotest, 2021). Most relevant for our study period 1959-2022 is the agricultural crop damage data archive by the Swiss agricultural hail insurance Schweizer Hagel. Sereal radar-based measurements complement the archive in later periods. The historical information is temporally and spatially resolved on a daily and municipality scale, respectively. From this, we derived a time series with binary hail YES / NO information using a threshold of 5 municipalities. The threshold was selected to best match the annually averaged haildays derived from POH data (see Sect. 3.1). It is important to note that this historical data archive is subject to significant uncertainties such as reporting biases, changing vulnerabilities and exposures of crop cultures, hail prevention measures, the fraction of insurance partition, merges of municipalities, and many more (see Willemse (1995)). Due to those limitations, the historic data cannot be interpreted as a homogeneous time series and a quantitative comparison is impossible. However, the data contains valuable information on

https://doi.org/10.5194/egusphere-2024-371
Preprint. Discussion started: 23 February 2024

the weakest and strongest active hail years as well as an indication of multi-year variability, which can complement model evaluation.

3 Methods

3.1 POH time series

To identify haildays in northern and southern Switzerland, this study uses daily POH data from 2002 to 2022 during the hail months of April to September. We here use the same domains and thresholds as Barras et al. (2021). The extent of the daily area of POH $\geq 80\%$ is extracted separately for the domains north and south of the Alps (Fig. 1). For a day to be categorized as a hailday, the daily maximum POH needed to equal or exceed 80% for at least 580 km^2 in the northern domain and 499 km^2 in the southern domain. Barras et al. (2021) found that these thresholds best correlate with days with car damage reported across Switzerland from 2002 to 2012. We tested the sensitivity of our model results to this threshold by varying the area threshold but did not find a significant impact on misses or false alarms, confirming earlier findings of low area threshold sensitivity (Madonna et al., 2018).

The above described methodology resulted in a total of 566 haildays in the northern region and 560 in the southern region between 2002 and 2022. The apriori probability is 14.7% in the north and 14.5% in the south, i.e. hail occurs on around 15% of days between 1 April to 30 September in both domains. Predicting rare convective events with statistical methods is often difficult due to their local mesoscale character, dynamic evolution over time, and, consequently, limited data (Davison and Huser, 2015; Hitchens et al., 2013). With the apriori probability of approx. 15% in our sample, hail on our domain is a comparatively frequent event, mitigating some of the statistical intricacies.

On average, 27 haildays per year occur in the north and 26.7 in the south. A maximum of 44 haildays was recorded in 2009 in the north and a maximum of 37 in 2018 in the south. A minimum of 16 haildays occurred in 2020 in the northern domain and a minimum of 17 haildays in the year 2007 in the southern domain.

There is considerable interannual variability with domain-specific differences during the observation period (see Fig. 2 (a,b)). While most recent years in the south show a frequency above the average, the opposite is true in the north. However, the time series of 20 years is too short to assess or interpret trends in a robust way.

Hail is a seasonal phenomenon with a strong annual cycle in both the northern and southern domains, as shown in Fig. 2 (c,d). Over all years, June has the most haildays in the north with 166 haildays, closely followed by July with a total number of 157. In the south, hail is most frequent in July, with 189 haildays. The POH hailday time series for the two study domains serve as the observational base reference for our model study.

https://doi.org/10.5194/egusphere-2024-371
Preprint. Discussion started: 23 February 2024

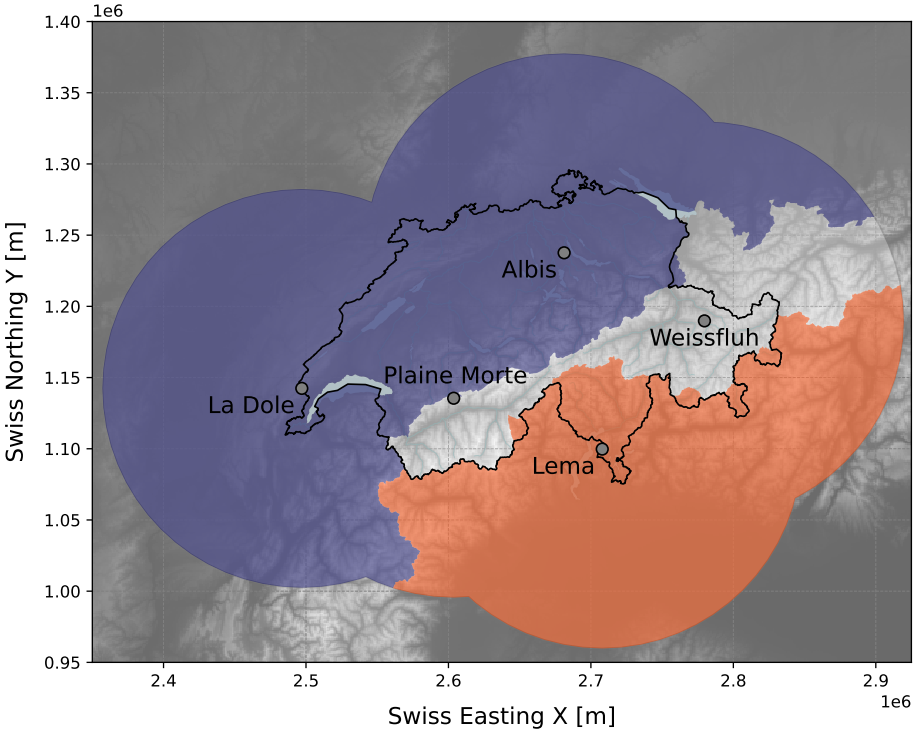

Figure 1. The study areas north of the Alps (blue) and south of the Alps (orange) within 140 km radius of the five MeteoSwiss weather radars (black circles) overlaid on a digital elevation map (gray shading, source: Federal Office of Topography swisstopo).

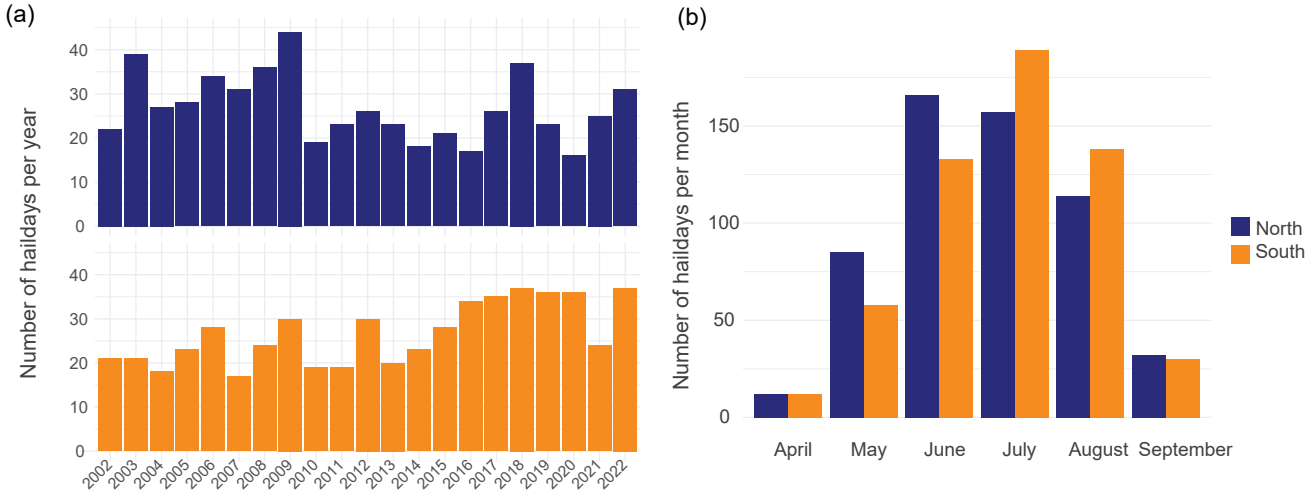

Figure 2. Total sum of yearly (a) and monthly (b) haildays for the northern (blue) and southern domains (orange) for 2002 to 2022.

https://doi.org/10.5194/egusphere-2024-371
Preprint. Discussion started: 23 February 2024

4 Model development and performance

4.1 Logistic regression

This work proposes the use of a multivariate technique to quantify the convective potential of the atmosphere. Applequist et al. (2002) suggests multiple logistic regression as an appropriate tool for such a binary classification problem, and logistic regression models have effectively been used in many studies to model the occurrence of hail- or thunderstorms (e.g., Billet et al. (1997); Sánchez et al. (2009); Schmeits et al. (2005); Battaglioli et al. (2023a)). With a multiple logistic regression model, we can predict the occurrence probability p of hail as a function of several different environmental parameters $(x_1, x_2, \ldots, x_n)$ as independent variables (Hosmer and Lemeshow, 2000). Typically, a binary variable (e.g., hail YES / NO) is defined as a dependent variable y. The occurrence probability $p(x)$ is defined as:

$$y = p(x) = 1/(1 + e^{(-g(x))}), \quad \text{where} \quad 0 \leq p(x) \leq 1. \tag{1}$$

The model is based on a linear regression:

$$g(x) = \beta_0 + \beta_1 \times x_1 + \beta_2 \times x_2 + ... + \beta_n \times x_n \tag{2}$$

The regression coefficients β_n are computed by R with the glm package by using the maximum-likelihood method. For model training and testing, the dataset was divided into training and test sets by splitting data points from 2012-2022 randomly into 70% and 30%. Additionally, we used the POH data from 2002 - 2011 for an independent validation set to prevent overfitting. To estimate the performance of the model, we used 10-fold cross-validation. A total of 75 different convective and meteorological parameters were tested as predictors x_n (see Table A2). The best models were chosen by comparing multiple performance metrics. We considered the Akaike Information Criterion (AIC), the Bayesian Information Criterion (BIC), the Critical Success Index (CSI, or threat score), the Probability of Detection (POD), the False Alarm Ratio (FAR), the Success Ratio (SR), Heidke Skill Score (HSS), the bias, precision and accuracy values. The metrics were mostly calculated manually from contingency tables by averaging over the 10 different test / training / validation data splits. Equations for contingency table metrics, AIC and BIC can be found in the appendix in Table A1. We use a combination of multiple metrics to build a model with the optimal balance between over- and underfitting, while holding the correct prediction of hits in slightly greater importance than false alarms, as finding haildays is our main priority. We also made sure to avoid multicollinearity between predictor variables by requiring the Variance Inflation Factor (VIF, Mansfield and Helms (1982)) of any predictor to remain below four.

In many studies, the common threshold value to differentiate between the occurrence of hail and no hail is $p(hail) \geq 0.5$ (Hosmer and Lemeshow, 2000; Sánchez et al., 2009; López et al., 2007). Some studies (e.g. Mohr et al. (2015a)) suggest a threshold closer to the apriori probability of the event. For hailday occurrences in our dataset, the apriori probability was approx. 15%. However, upon closer examination, we found that the number of events is heavily overestimated with a threshold similar to this. The optimal threshold of $p(hail) \geq 0.4$ for the north and $p(hail) \geq 0.44$ for the south was found by looking at ROC curves as well as plots modelled vs. observed haildays .

https://doi.org/10.5194/egusphere-2024-371
Preprint. Discussion started: 23 February 2024

To examine whether we obey the necessary assumptions for logistic regression, we next checked for extreme outliers as well as for the linear relationship between the explanatory variables x_n and the logit of the response variable y. Some variables did not have a perfect linear relationship, e.g. CAPE, which is probably one reason why it was not chosen as a predictor for the final logistic regression models. We also build GAM´s to allow for non-linear relationships and interactions that might be poorly fitted in the logistic regression models (see Sect. 4.2).

Additionally, a residual analysis was done to ensure no systematic errors were still present in the model residuals. We looked at the yearly and monthly averaged residuals of the ten training and test data folds separately. A strong increase in the variance of yearly residuals was present with data points before 2012, which warranted our decision to only use POH data from 2012 onwards for training. In 2012, there was a major update to the Swiss radar network. Even though we reduced the size of the training dataset, the predictive skill of the models for both domains increased slightly. Furthermore, we introduce a categorical variable $month$ as an additive factor in both models, containing the six considered months of April through September. This aimed to reduce the non-stationarities associated with a seasonal cycle. Again, residuals were more regular after, and the model´s predictive skill increased.

Various other methods to address non-stationaries and long-term trends in the data were discussed, such as anomalies for detrending or seasonal correction, but eventually did not lead to satisfactory results. The trend can also not be estimated apriori from the short observations and, hence, cannot be excluded in the models.

To find the optimal number of predictors, we applied a manual stepwise forward method, resulting in a final number of five predictors plus the factor $month$ for both the northern and southern models. The respective best logistic models are:

$$g(hail) = \beta_0 + \beta_1 \times LI + \beta_2 \times TT + \beta_3 \times OMEGA\_vint + \beta_4 \times Q\_vint + \beta_5 \times BI + \sum_{n=5}^{9} \beta_n \times 1_{month=n+1} \quad (3)$$

for the northern model and

$$g(hail) = \beta_0 + \beta_1 \times LI + \beta_2 \times kx + \beta_3 \times v\_500 + \beta_4 \times sp\_mean + \beta_5 \times TT + \sum_{n=5}^{9} \beta_n \times 1_{month=n+1} \quad (4)$$

for the southern model. The threshold for identifying a hailday was set to $p(hail) \geq 0.4$ for the north and $p(hail) \geq 0.44$ for the south. LI is the Surface Based Lifted Index. TT is the Total Totals Index, $OMEGA\_vint$ is the vertically integrated vertical velocity, Q_vint is the vertically integrated specific humidity, BI is the Boyden Index, kx is the K-Index, v_500 is the meridional component of the wind at 500 hPa and sp_mean is the mean surface pressure. All descriptions and the mean values and percentiles of all variables can be found in the appendix in Table A2 and Table A3. A detailed evaluation of the final ensemble model performance is done in Sect. 4.3. Here we discuss the respective performance skills for the separate logistic models summarized in Table 2. The northern model has a higher POD and lower FAR, as well as a lower CSI than the southern model. This suggests that the northern model can overall better distinguish between hail and no haildays and that it misses fewer haildays than the southern model. Nonetheless, when comparing our models to other studies we rank either better with a lower FAR (e.g. all studies mentioned in Raupach et al. (2023a), or similar to other studies like in López et al. (2007) and Gascón et al. (2015). All coefficients and respective p-values of the covariates are listed in Table 1.

https://doi.org/10.5194/egusphere-2024-371
Preprint. Discussion started: 23 February 2024

All model predictors except the categorical factor month are (highly) significant. Although insignificant, the model´s performance decreased when removing the factor $month$. Possible explanations for the months not being significant in our model could be that our sample size is too small for the effect to become significant or that there is multicollinearity between months in the model.

Only LI and TT show up in both models, albeit with different coefficients, while all other covariates differ for both models. Z-values in Table 1 show that instability and moisture predictors (LI, kx, Q_vint) have the highest feature importance in both models. While LI has the highest absolute z-value in both models, the southern model imputes higher importance compared to the models other predictors´ z-values. In the north, the BI has the second highest z-value. The z-value measures how many standard deviations the coefficients are from zero, hence the higher the absolute value, the higher the importance.

To illustrate the modelled relationship between response and predictors graphically, Fig. 3 and 4 show marginal response plots of the logistic models. In both figures, the response is plotted against each independent model covariate x_n and against the linear combination of all covariates (bottom right graph) with loess smooth functions. The model, as represented by the red dashed line, clearly match the marginal relationships of the data represented by the solid blue lines. This indicates that all predictors are well fitted and do not need further modification. The grey points show the distribution of covariates. Important to mention is, that some variables have a stronger influence on the model's predicted probability than others. A LI of $-5K$ already translates to a probability of hail of 60%, while the highest probability of any $OMEGA\_vint$ value reaches less than 30% (see Fig. 3). In all models, there were two to three variables that mainly defined the hail occurrence probability, while the remaining two were used for "finetuning". A short summary of how each chosen model predictor is connected to hail favouring environments is following. The Surface Based Lifted Index (LI) is a measure of stability of the atmosphere and is defined as the temperature difference of a parcel that is lifted from the surface to its LCL dry adiabatically and further pseudo-adiabatically to 500hPa. A Negative LI represents atmospheric instability, which is favourable for the development of strong updrafts within convective storms. The higher the absolute value of the negative LI the more unstable is the atmosphere (hailstorms possible at LI of approx. $-4K$ (Kunz, 2007)). This matches the models fitted negative linear relationship in both regions (see Fig. 3 and Fig. 4.

The Total Totals Index (TT) combines two components, the Vertical Totals (VT) and the Cross Totals (CT). The VT reflects static stability or the lapse rate between 850 and 500 hPa. The CT includes the 850 hPa dewpoint. As a result, TT increases with increasing static stability and 850 hPa moisture, but it would be unrepresentative in situations where the low-level moisture lays below the 850 hPa level. Additionally, convection may be inhibited despite a high TT value if a significant capping inversion is present. A TT of $50K$ or larger usually translates to hailstorms being possible (Mohr and Kunz, 2013). In the northern and southern models, the probability of hail exceeds 50% with TT values of approx. $52K$.

The K-Index (kx), like the VT, is based on the vertical temperature gradient between 850hPa and 500hPa. Higher humidity in 850hPa, expressed by higher dewpoint temperature at 850hPa, increases kx. Furthermore, lower humidity in higher levels (700 hPa) decreases the chance of thunder- or hailstorms to occur. The higher the kx the higher the probability for a hailstorm. kx above $20-30K$ usually indicates possible thunder- or hailstorms (Kunz, 2007), which matches our relationship of kx to hail in the southern model.

https://doi.org/10.5194/egusphere-2024-371
Preprint. Discussion started: 23 February 2024

The Boyden Index (BI) was originally developed to assess the thunderstorm risk at frontal passages. This convective parameter does not include information on humidity, but only on the temperature at 700hPa and the thickness of the 1000-700hPa level (which is also proportional to its temperature). The higher the value of the BI, the greater the risk of thunderstorms. The threshold value for thunderstorms to develop is approximately 95 (Boyden, 1963), which is a bit higher than what the model learns for the northern region (50% probability of hail at BI greater than approx. 90). As mentioned in Sect. 1, on the northside of the Alps, around 20-40% of Swiss hailstorms are associated with fronts, which is probably why that parameter was chosen and why it has high importance in the model. The vertically integrated vertical velocity ($OMEGA\_vint$) represents the vertical motion of air within the full column of the atmosphere. Negative values of $OMEGA\_vint$ indicate upward motion of air, which is crucial for the development of thunder- and hailstorms. Highly negative values of ($OMEGA\_vint$) indicate very strong lifting, potentially with a very strong and narrow updraft. However, we do not see the highest probabilities for hail for those cases, but rather for median $OMEGA\_vint$ values (see 3). In the context of hail formation, this could mean that a less intense and wider updraft is more favourable than a very strong and narrow one, where hail embryos could be ejected prematurely, as already modelled by Lin and Kumjian (2022).

The vertically integrated specific humdidity (Q_vint) reflects the total amount of water vapor available for hailstorms to develop and hence, the larger Q_vint, the higher the probability of a hailstorm.

Lastly, v_500, the meridional component of the wind at 500 hPa and the mean surface pressure (sp_mean) might be connected to hailstorm development indirectly. In the pre-storm environment, a drop in surface pressure can indicate the presence of a low-pressure system, which typically signifies the approach of a weather disturbance or frontal boundary. However, in our model we see that the highest probabilities for hail are achieved neither with very high nor very low pressure (see Fig. 4). v_500 might indirectly represent wind shear. Wind shear, which is the change in wind speed and direction with height, is important for the organization and persistence of the storm system, specially for those capable of producing hail. A positive sign of v_500 indicates air moving towards the north at 500 hPa, which the model translates to higher probabilities for hail. This might also be related to the synoptic situation in the south of Switzerland, where moist, warm air is often advected from the Mediterranean (Schemm et al., 2016).

All the mentioned connections are part of a complex interplay of atmospheric conditions that contribute to hailstorm development. This is why we examine a combination of various parameters, including those related to instability, moisture, and wind patterns, to assess the likelihood of hailstorms in a synergy in our models.

Automatic predictor selection procedures (e.g. Recursive feature importance, LASSO, etc.) gave worse performing models than a manual stepwise approach combined with expert knowledge that was based on earlier considerations on optimal distribution separations of hail vs. no haildays (see Trefalt (2017)) and computed correlations (see Fig. A1, Fig. A2 and Table A4). Further discussions on the variable selection and their importance will follow in Sect. 6, however, it is important to differentiate between the two domains. When applying the combination of variables of the model north on the region south and vice versa, the coefficients changed and the predictive skill declined. This again justifies the use of an individual combination of predictors for each region, rather than applying one model for the whole area of Switzerland.

https://doi.org/10.5194/egusphere-2024-371
Preprint. Discussion started: 23 February 2024

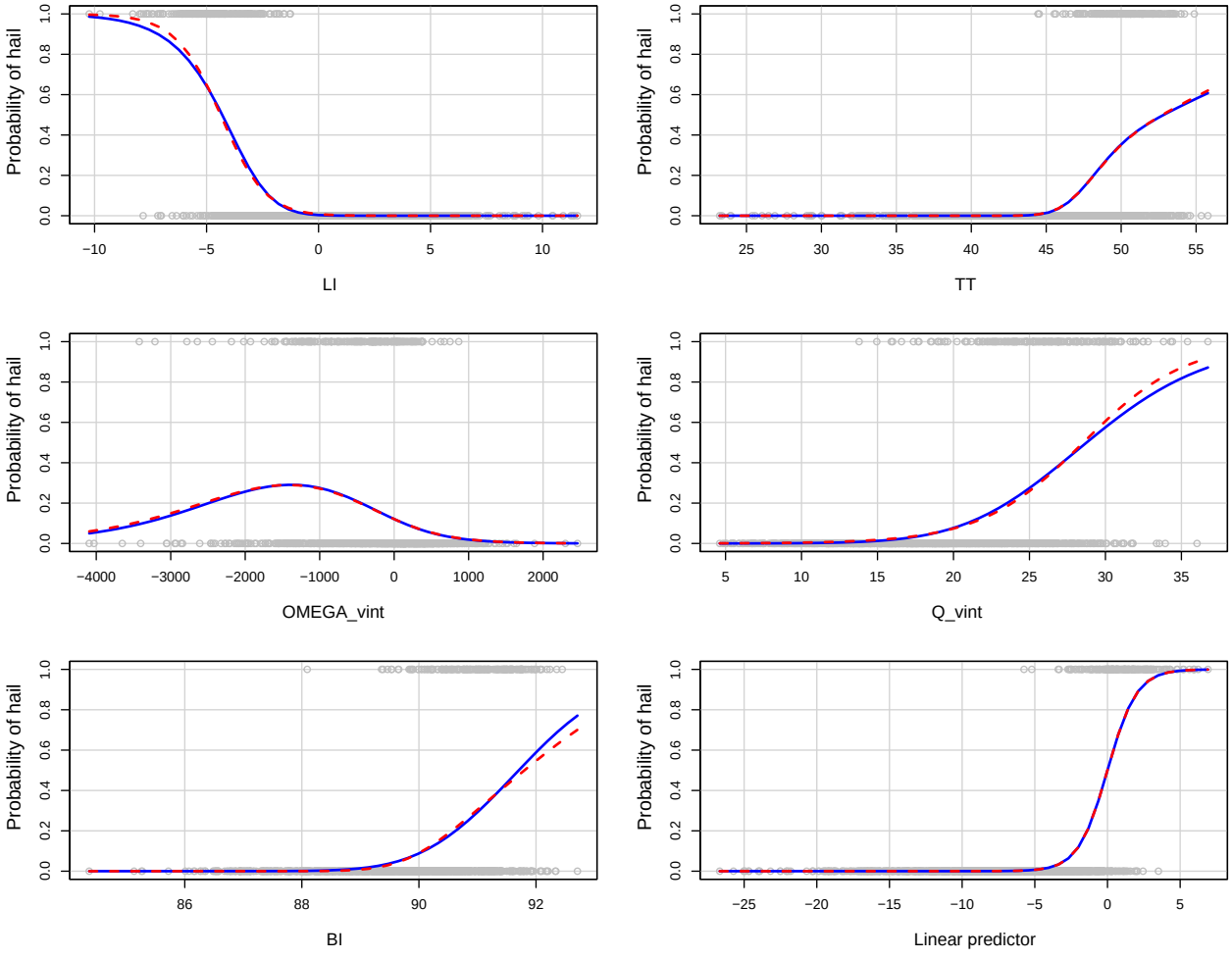

Figure 3. Marginal model plots showing the modelled relationship of each covariate (x-axes) to the modelled probability of a hailday (y-axes). The bottom right graph shows the linear combination of all covariates. The model is represented by the red dashed line, and the marginal relationships of the data is represented by the solid blue lines. The grey points show the distribution of covariates. Some variables have a stronger influence on the model's predicted probability than others.

https://doi.org/10.5194/egusphere-2024-371
Preprint. Discussion started: 23 February 2024

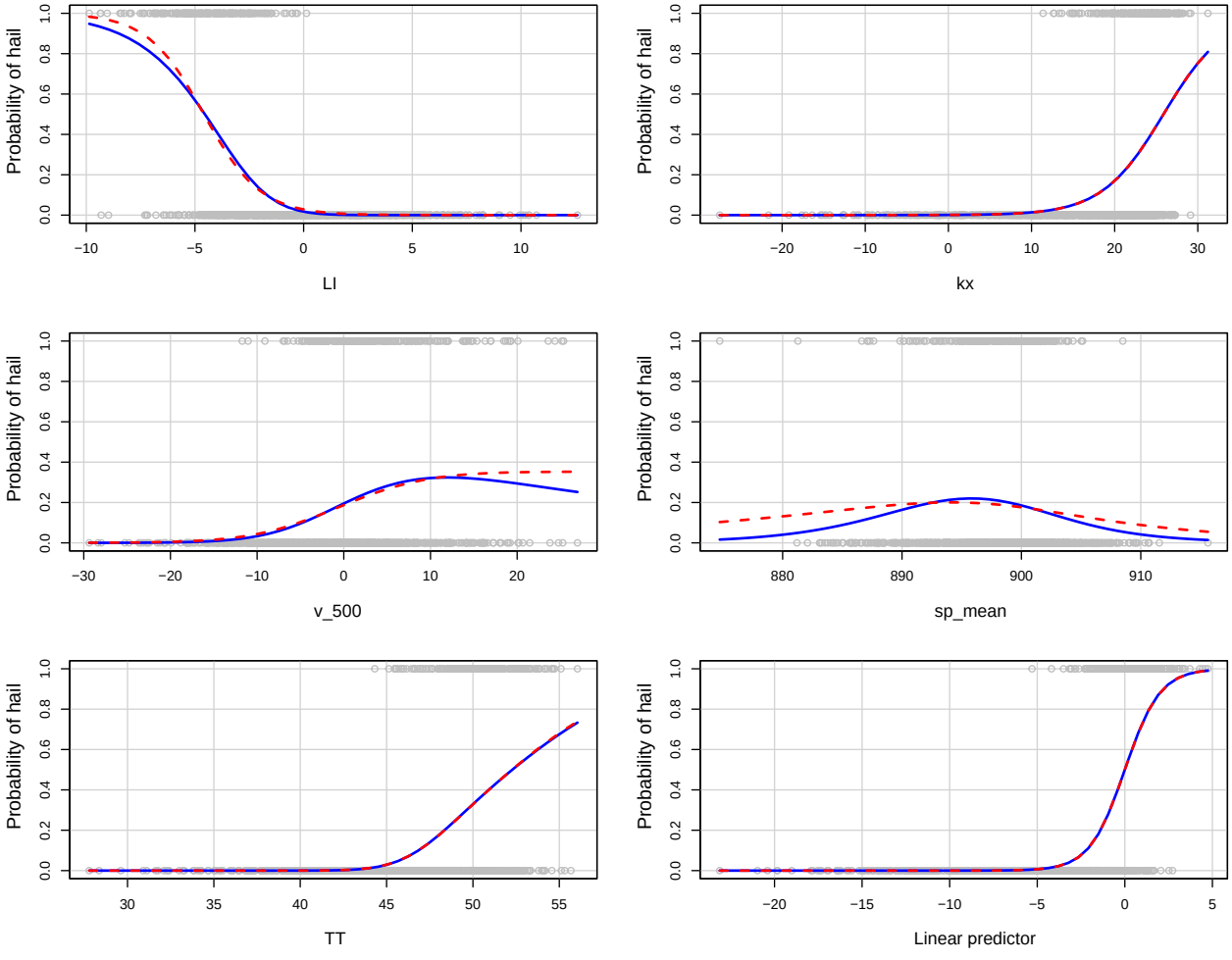

Figure 4. As Fig. 3, but for the southern region.

https://doi.org/10.5194/egusphere-2024-371
Preprint. Discussion started: 23 February 2024

Table 1. Coefficients, standard errors, z-values and p-values of all covariates of the logistic regression model north and south. Positive (negative) signs indicate a positive (negative) relationship of the quantitative predictors with modelled hail occurrence and with hail occurrence relative to the reference category (April) for the categorical predictors. Asterisks indicate significance levels of the p-values * 0.01, ** 0.001, *** 0.000.

Covariate North	**Estimate**	**Std. Error**	**z value**	$\mathbf{Pr}(>\|\mathbf{z}\|)$
(Intercept)	-37.20	4.34	-8.57	$< 2 \times 10^{-16}$ ***
LI	-0.71	0.12	-6.22	5.11×10^{-10} ***
TT	0.39	7.95×10^{-2}	4.93	8.44×10^{-7} ***
OMEGA_vint	-6.38×10^{-4}	2.02×10^{-4}	-3.15	1.61×10^{-3} ***
Q_vint	0.24	0.05	5.17	2.35×10^{-7} ***
BI	0.10	0.02	5.65	1.62×10^{-8} ***
factor(month) 5	0.90	0.80	1.07	0.29
factor(month) 6	0.07	0.84	0.08	0.94
factor(month) 7	-0.48	0.89	-0.55	0.58
factor(month) 8	-0.78	0.91	-0.87	0.39
factor(month) 9	-1.54	0.94	-1.63	0.11
Covariate South	**Estimate**	**Std. Error**	**z value**	$\mathbf{Pr}(>\|\mathbf{z}\|)$
(Intercept)	72.89	25.21	2.89	3.84×10^{-3} **
LI	-0.65	0.08	-7.87	3.60×10^{-15} ***
kx	0.15	0.03	4.50	6.73×10^{-6} ***
v_500	0.07	0.02	3.97	7.29×10^{-5} ***
sp_mean	-0.10	0.03	-3.54	3.94×10^{-4} ***
TT	0.18	0.06	3.13	1.77×10^{-3} **
factor(month) 5	-0.21	0.52	-0.41	0.68
factor(month) 6	0.02	0.55	0.04	0.96
factor(month) 7	-0.30	0.61	-0.50	0.62
factor(month) 8	-0.16	0.59	-0.27	0.77
factor(month) 9	-1.27	0.63	-2.01	0.04 *

4.2 Generalized Additive Models (GAM)

As mentioned before, the use of a Generalized Additive Model (GAM) was warranted to account for potential non-linear and non-parametric correlations in the data that may not be adequately captured by a conventional logistic regression. The goal was also to find a more "simple" model with fewer composite parameters, facilitating enhanced interpretability while maintaining or even improving performance. A generalized additive model (GAM) is a generalized linear model in which the linear response variable depends linearly on the smooth functions of the models' predictor variables (Hastie and Tibshirani, 1987). The logistic

https://doi.org/10.5194/egusphere-2024-371
Preprint. Discussion started: 23 February 2024

Table 2. Performance metrics of the logistic model north and south. Metrics are calculated from k-fold cross-validation and are the averages of the test datasets. For POD, CDI, HSS, AUROC, Bias, Precision and Accuracy a value close to 1 indicates good performance, while FAR, AIC and BIC should remain as low as possible.

Metric	North	South
POD	0.76	0.57
FAR	0.22	0.35
CSI	0.62	0.44
HSS	0.73	0.53
AUROC	0.86	0.87
Bias	0.98	0.88
Precision	0.78	0.65
Accuracy	0.94	0.86
AIC	421.19	651.65
BIC	477.90	708.34

equation from before (see Eq. 2) becomes:

$$g(x) = \beta_0 + f_1(x_1) + f_2(x_2) + ... + f_n(x_n) \tag{5}$$

The nonparametric form of the functions f_n enhances the flexibility of the model, but it also imposes constraints on additivity, allowing us to interpret the model in a similar manner as the multiple logistic regression. $CAPE$ showed up more often as a model predictor in the GAM´s than in the logistic regression models during model training. Nevertheless, the best model for the northern domain preferred LI over $CAPE$. The selection of predictors followed the same procedure as in the logistic regression model, however, for every variable that presented an effective degree of freedom (edf) > 1 a smoothing spline function was used to allow for non-linear effects. The model fitting was done using the R package mgcv. In the GAM´s, we again introduced a $factor(month)$ as a categorical variable, and exclusively used data from 2012 onwards to train the model.

The best GAM in the northern domain is:

$$g(x) = \beta_0 + f_1(LI) + f_2(kx) + f_3(TT) + f_4(deg0l) + f_5(WS\_06) + f_6(WS\_36) + \sum_{n=5}^{9} \beta_n \times 1_{month=n+1} \tag{6}$$

And for the southern domain:

$$g(x) = \beta_0 + f_1(CAPE) + f_2(WS\_06) + f_3(d2m) + f_4(TT) + f_5(w\_500) + \sum_{n=5}^{9} \beta_n \times 1_{month=n+1} \tag{7}$$

The threshold for identifying a hailday was set to $p(hail) \geq 0.4$ for the north and $p(hail) \geq 0.41$ for the south. Here LI is the Surface Based Lifted Index, kx is the K-Index, TT is the Total Totals Index, $deg0l$ is the freezing level, $CAPE$ is the most

https://doi.org/10.5194/egusphere-2024-371
Preprint. Discussion started: 23 February 2024

unstable convective available potential energy, WS_06 is the magnitude of bulk wind shear between 10m and 6km, WS_36 is the magnitude of bulk wind shear between 3km and 6km, $d2m$ is the 2m dewpoint temperature, w_500 is the vertical velocity at 500 hPa. The last five variables do not show up in the logistic regression models.

In the models, a combination of $CAPE$ and TT (south) or LI and TT (north) lead to a strong increase in the performance of the model. Hence, we still allowed composite parameters like TT in favor of a better predictive performance. The performance skills for the GAMs can be found in Table 5. Both GAM´s perform very similarly to the logistic regression models. The northern GAM outperforms the southern model. Table 3 provides the coefficients and their corresponding p-values for parametric covariates, while Table 4 details the non-parametric terms. Again, all model predictors except the $factor(month)$ are (highly) significant. The models' explained deviance is 63.1% for the north and 45.5% for the south.

We can visualize the modelled relationship between the response and the covariates once again, while reflecting how each covariate is connected to hailstorm development. Figures 5 and 6 depict partial dependence plots for both Generalized Additive Models (GAM´s). Each figure illustrates the partial effect of individual model covariates x_n on the probability of having a hailday. The black vertical lines represent the distribution of the covariates, while the black horizontal lines denote smoothing functions with varying degrees of freedom that capture the modelled relationships. The red horizontal lines are the y = 0 lines, separating the plot space into positive and negative partial effect. For interpretation, we will go trough each model separately.

In the southern model, the partial effect on the probability of hail is positive with a $TT \geq 4K$, with negative w_500, with a $d2m \geq 282K$, with $WS\_06 \geq 10ms^{-1}$ and $CAPE \geq 100Jkg^{-1}$. $CAPE$ is a measure for the energy available for convection. Large positive values of $CAPE$ indicate that an air parcel would be much warmer than its surrounding environment and therefore, very buoyant. In the context of hail, high $CAPE$ values signify that strong updraft speeds can occur within thunderstorms, allowing for the sustained lifting of moist air to colder altitudes where hailstones can form and grow. Observed values in thunderstorm environments often may exceed 1000Jkg^{-1}, however, in Europe severe hailstorms also occur with less $CAPE$ (Taszarek et al., 2020a). In our model we see a strong positive effect of $CAPE$ already at values of approx. $500Jkg^{-1}$. The slope of the curve then declines towards larger values, suggesting that more $CAPE$ does not always lead to higher potential for hail, but that it is rather maximized for an intermediate range of $CAPE$. This relation has also been found by Lin and Kumjian (2022). WS_06 has a very similar relation in the southern model, where at least $10ms^{-1}$ is needed for a positive effect, but then only increases slightly with increasing magnitude of deep level shear. Again, shear does have the least importance in the model, compared to the other predictors. The dewpoint temperature at 2m ($d2m$) assesses the moisture availability near the surface. Higher dewpoint temperatures imply more moisture in the air, which is necessary for the formation of hail stones by condensation and freezing in the updraft. Additionally, the release of latent heat due to condensation of moisture enhances buoyancy, fostering the development of strong updrafts necessary for hail formation. In our model we see the highest partial effect for hail occurrence with the highest dewpoint temperatures. Similar to the vertically integrated vertical velocity $OMEGA\_vint$, the vertical velocity at 500 hPa (w_500) is a measure for the vertical motion of air, here for the layer at 500 hPa. Negative values indicate an upward motion and hence measure updraft strength. The highest positive effect is achieved with the strongest negative vertical velocities.

https://doi.org/10.5194/egusphere-2024-371
Preprint. Discussion started: 23 February 2024

In the northern model, the partial effect on the predicted probability of the model is positive when $LI \leq 0K$, $TT \geq 45K$, $kx \geq 15K$. We already explained the relationship of LI, kx and TT to hailstorm development in Sect. 4.1. The GAM´s fit similar linear relationships than the logistic regression models, with higher probabilities of hail achieved with increasing kx and TT and decreasing LI. Notably, the deep layer shear WS_06 exhibits a non-linear relationship to the response variable. For instance, WS_06 has its most negative effect at values around $0 - 10ms^{-1}$, transitioning to a positive effect from around $15ms^{-1}$. The curve's slope declines noticeably in the presence of very high wind shear values, suggesting again that higher bulk shear does not always lead to a further increase in the probability of hail. Additionally, confidence intervals of the smoothing functions widen significant towards the tails of each covariate distribution. In GAM's we are not limited by multicollinearity between model terms, which is why both WS_36 and WS_06 were able to appear in the northern model. The model seemed to prefer including both WS_36 and WS_06 over just one of them, as the individual predictor otherwise became non-significant and less important. Surprisingly, WS_36 has a negative linear relationship to hail. To gain a deeper understanding of how the model terms WS_36 and WS_06 interact, we further examined contour plots depicting conditional probabilities based on pairs of model predictors (not shown). The highest probabilities of hail are achieved with high WS_06 but low WS_36 in the northern model. Typically the difference in 3km to 6km is much smaller than the deep layer shear WS_06. Hence, the model might indirectly learn, that the low-level inflow (0-3km) are more important to hail growth (and storm dynamic, as the inflow dominates storm dynamic) than the 3-6km layer shear. High 3-6km wind shear rather influences the stretching of the hodograph, making for stronger storm relative winds, and impacting downdraft formation and storm motion. With strong storm relative winds, the hail embryos might also be ejected out of the hail growth zone too quickly to experience significant growth (Dennis and Kumjian, 2017). This could explain why the model learns that high shear at this level leads to less probability of hail when differentiating between hail and no hail (and not hail size). We also need to mention, that we are just taking into account bulk shear which doesn´t include the curvature of the hodograph and the rotation of the storm. Dennis and Kumjian (2017) show that the biggest hail growth volume is achieved with a straight, long hodograph because of a strong and in the shear direction elongated updraft, rather than with a curved hodograph.

Lastly, the freezing level $deg0l$ is indicative of the altitude at which freezing occurs in a thunderstorm. A lower freezing level may translate to a higher potential for hail formation because of the longer hail growth zone where embryos are circulating through areas of high supercooled liquid water and are able to grow bigger. However, the model fits an opposite relation. The highest probabilities of hail are achieved at freezing levels between 2500m.a.g.l. and 3500m.a.g.l.. A negative linear relationship is evident among freezing levels below $2500,$m.a.g.l., indicating that lower values of $deg0l$ correspond to a reduction in hail probabilities and not an increase. This unambiguous relation has also been seen by Kunz (2007) before. This might suggest, that our model does not learn about the melting or growing of the hail embryos from the freezing level, but that it is connected to the height of the cloud base and therefore the width of the updraft (Mulholland et al., 2021).

Plotting conditional probabilities for hail based on the different predictors (not shown), implies that WS_06, WS_36 and $deg0l$ has very low importance in the model than SLI and TT.

https://doi.org/10.5194/egusphere-2024-371
Preprint. Discussion started: 23 February 2024

The partial dependence plots offer insights into how the model derives probabilities through combined model effects. The thresholds of positive and negative partial effects are specific to each model's *combination* of predictors within the selected domain and should only be used for model output statistics under the same constraints.

https://doi.org/10.5194/egusphere-2024-371
Preprint. Discussion started: 23 February 2024

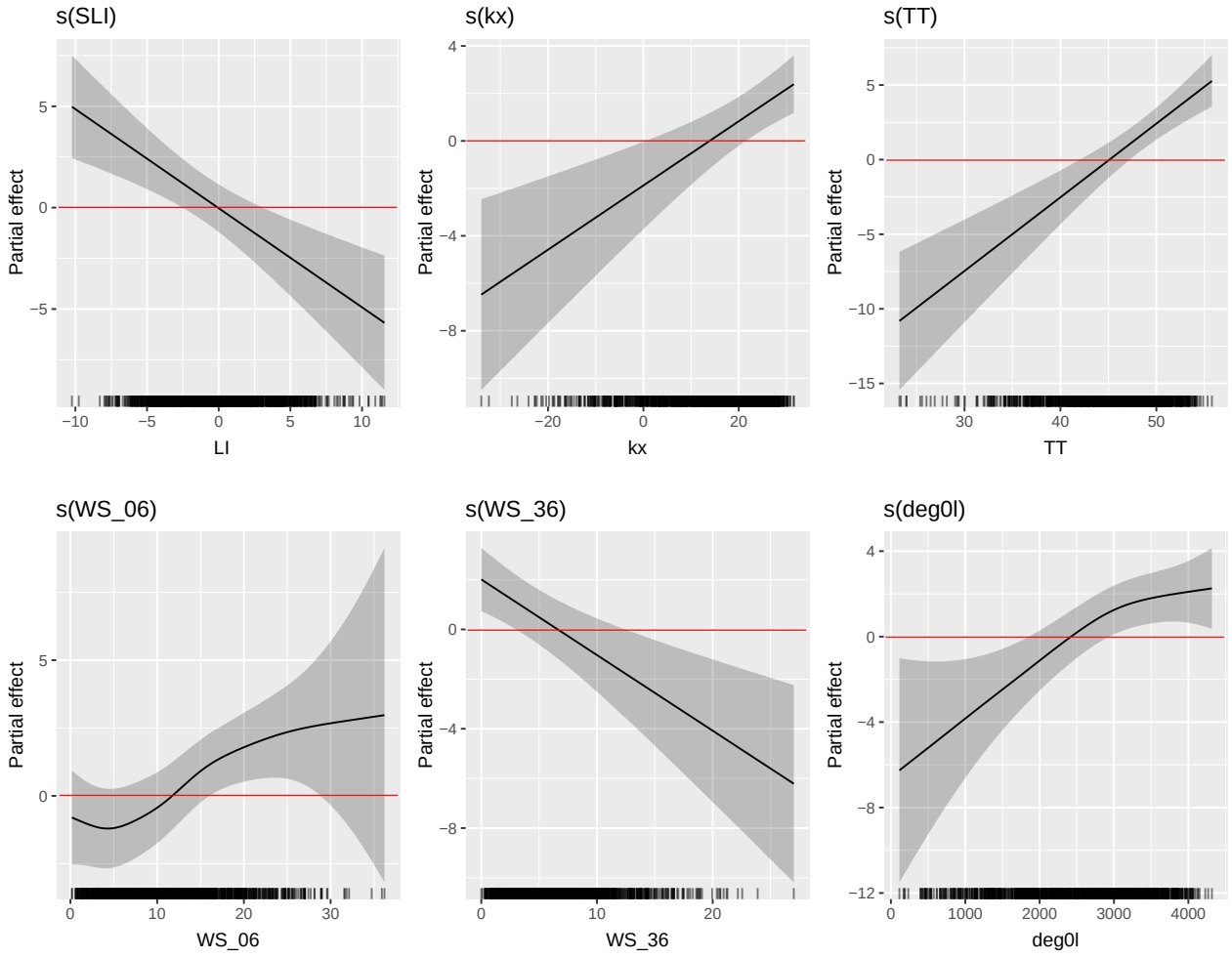

Figure 5. Partial dependence plots for each model covariate in the northern model. The black solid line plus grey uncertainty range represents the modelled partial effect of the covariate to the response. The red $y = 0$ lines separate positive from negative effects. The short black vertical lines indicate the covariate distribution.

https://doi.org/10.5194/egusphere-2024-371
Preprint. Discussion started: 23 February 2024

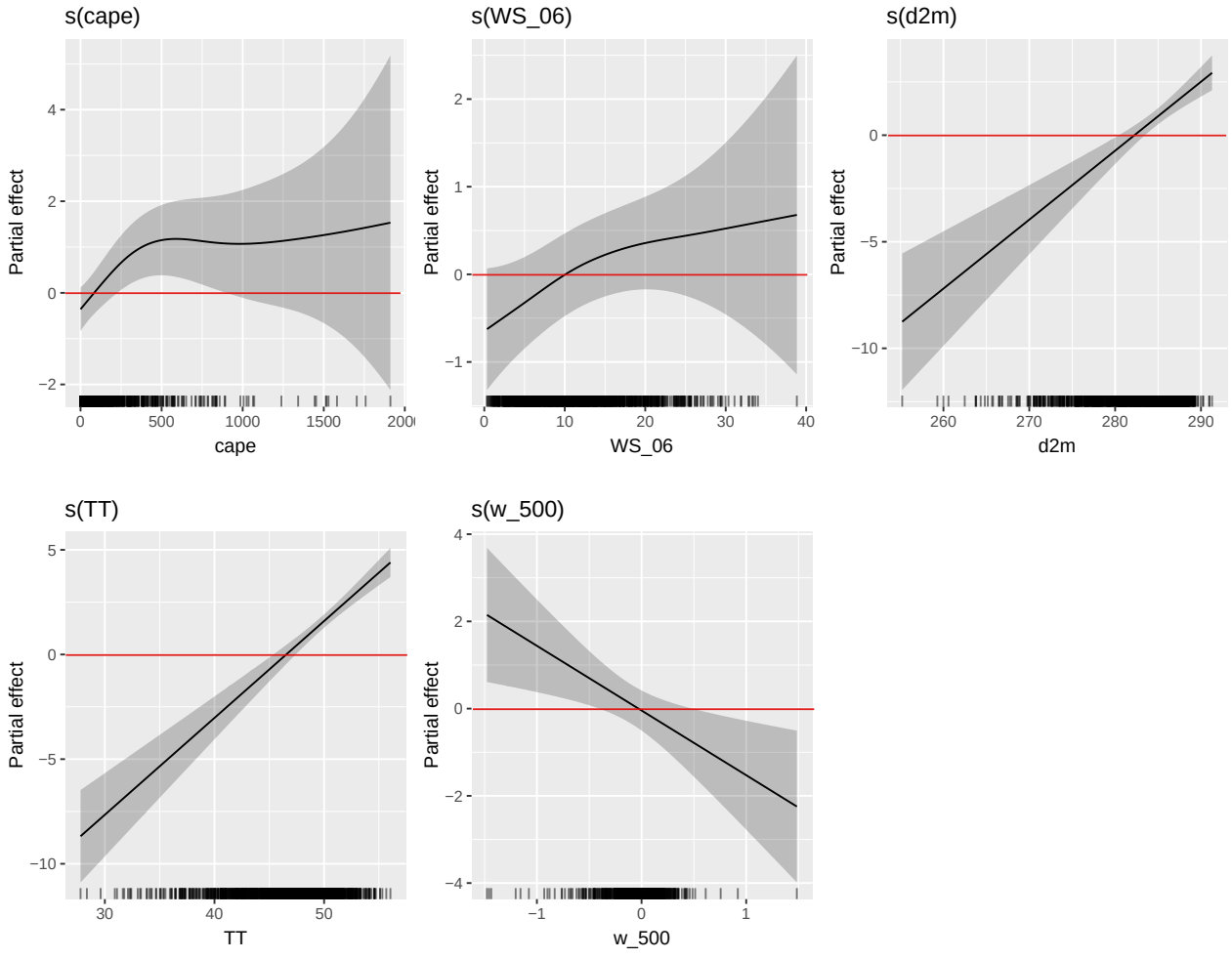

Figure 6. Same as Fig. 5 but for the southern model.

https://doi.org/10.5194/egusphere-2024-371
Preprint. Discussion started: 23 February 2024

Table 3. Coefficients, standard errors, z-values and p-values of all non-parametric covariates of the GAM north and south. Positive (negative) signs indicate a positive (negative) relationship of the quantitative predictors with modelled hail occurrence and with hail occurrence relative to the reference category (April) for the categorical predictors. Asterisks indicate significance levels of the p-values * 0.01, ** 0.001, *** 0.000. Other non-parametric terms are found in Table 4.

Covariate North	**Coefficient**	**Std. Error**	**z value**	$\mathbf{Pr}(>\|\mathbf{z}\|)$
(Intercept)	-28.51	4.55	-6.27	3.53×10^{-10} ***
LI	-0.49	0.13	-3.90	9.74×10^{-5} ***
kx	0.14	0.04	3.84	1.23×10^{-4} ***
TT	0.49	0.09	5.37	7.71×10^{-8} ***
WS_36	-0.30	0.08	-3.60	3.14×10^{-4} ***
factor(month) 5	0.63	0.87	0.73	0.47
factor(month) 6	-0.40	0.91	-0.44	0.66
factor(month) 7	-0.99	0.97	-1.02	0.31
factor(month) 8	-1.26	0.98	-1.28	0.20
factor(month) 9	-2.14	1.00	-2.13	0.03 *
Covariate South	**Coefficient**	**Std. Error**	**z value**	$\mathbf{Pr}(>\|\mathbf{z}\|)$
(Intercept)	-115.67	16.22	-7.13	9.96×10^{-13} ***
d2m	0.32	0.06	5.87	4.38×10^{-9} ***
TT	0.46	0.05	9.16	$< 2 \times 10^{-16}$ ***
w_500	-1.48	0.54	-2.73	0.01 **
factor(month)5	-0.29	0.51	-0.56	0.58
factor(month)6	-0.25	0.55	-0.46	0.65
factor(month)7	-0.84	0.61	-1.38	0.17
factor(month)8	-0.87	0.61	-1.42	0.15
factor(month)9	-1.78	0.64	-2.78	0.01 **

https://doi.org/10.5194/egusphere-2024-371
Preprint. Discussion started: 23 February 2024

Table 4. Significance of non-parametric smooth terms in the GAM north and GAM south. edf are the effective degrees of freedom, Ref.df. are the residual degrees of freedom, Chi.sq. is the Chi-Square statistics. Asterisks indicate significance levels of the p-values * 0.01, ** 0.001, *** 0.000.

Covariate North	**edf**	**Ref.df.**	**Chi.sq**	**p-value**
s(WS_06)	3.70	4.63	20.67	7.66×10^{-4} ***
s(deg0l)	2.24	2.88	21.14	9.94×10^{-5} ***
Covariate South	**edf**	**Ref.df.**	**Chi.sq**	**p-value**
s(CAPE)	2.75	3.45	17.79	9.54×10^{-4} ***
s(WS_06)	1.64	2.06	8.37	1.65×10^{-2}*

Table 5. Performance metrics of the GAM north and south. Metrics are calculated from k-fold cross-validation and are the average of the test datasets. For POD, CDI, HSS, AUROC, Bias, Precision and Accuracy a value close to 1 indicates good performance, while FAR, AIC and BIC should remain as low as possible.

Metric	**North**	**South**
POD	0.76	0.61
FAR	0.23	0.36
CSI	0.62	0.45
HSS	0.73	0.55
AUROC	0.85	0.75
Bias	0.99	0.96
Precision	0.77	0.63
Accuracy	0.94	0.88
AIC	410.38	675.65
BIC	493.41	744.34

4.3 Ensemble model

For the final time series, we build an ensemble model out of the best logistic regression and GAM for each domain. With this, we aim to even out any leftover residual errors for a "best" final model that represents Swiss hail occurrences. The ensemble was produced by averaging the predicted probabilities for each method for each day and then using the mean threshold of both methods of $p(hail) < 0.4$ for the northern model and $p(hail) < 0.42$ for the south.

For analysing the performance of the ensemble model, we will focus on evaluating the model's ability to reproduce hail occurrence and its variability and seasonal cycle. Figure 7 (a,b) shows the per year and month aggregated haildays from the model (blue and orange lines) and from the POH time series (grey lines) over the period 2002 to 2022 for the northern domain (a) and the southern domain (b). In both regions, the lines overlap for a large part, which means that the inter- and intra-

https://doi.org/10.5194/egusphere-2024-371
Preprint. Discussion started: 23 February 2024

annual variability is well reproduced by the model. Upon closer examination, a more pronounced mismatch becomes apparent for the period 2002-2011 for both regions. As we decided to exclude this data due to biases in the earlier POH data, this was not surprising. Figure 8 (a,b) presents scatterplots of the haildays per month and year of the model plotted against POH for the northern domain (left) and the southern domain (right) for the whole period of 2002-2022 (and not just 2012-2022). Linear regression lines (colored lines), diagonal $x = y$ lines (black), and boxplots showing the distribution of each time series (below y- and x-labels) were added to compare the model's ability to reproduce the POH distribution. Generally, we see large inter- and intra-annual variability in the skill of the statistical model to predict haildays, as some years and some months are better predicted than others. The models tend to underpredict slightly in months with a lot of haildays. However, the overall correlation between the haildays per month and year of POH and the model is satisfactory, with 0.91 for the north and 0.87 for the south. We also compared performance for only the years 2012 - 2022 and not the whole 2002 - 2022 period, giving us slightly better values.

Figure 7 (c,d) depicts the total monthly sum of haildays of the models (colored curves) against the total monthly sum of haildays of POH (grey curves). The match of the lines suggests our model can reproduce the seasonal pattern in both regions well. We see a typical seasonal pattern with very few haildays at the beginning and end of the hail season and a strong increase during the warm summer months. The peak of haildays is more prominent in the southern domain (d) and appears mainly in July and in the north in June and July (c). The difference in peaks justifies again the use of two separate models to account for the differences in hail frequency. Fig. 8 (c,d) displays scatterplots similar to Fig. 8 (a,b), but here for the monthly sum of haildays of the model against the POH for the northern domain (c) and the southern domain (d). Similar results can be seen here, however, in months with fewer haildays, the models tend to underpredict slightly in both regions. The correlation between the monthly sum of haildays of the model and the POH is 0.99 for the north and 0.98 for the south.

The predictive skill of the models compares well to similar studies (see a comparison of performance metrics of different studies in Raupach et al. (2023a)). Figure 9 represents the models´ skill in a performance diagram showing the POD (left y-axis), SR (lower x-axis), CSI (labeled solid contours), and bias scores (labeled dashed lines) (diagram by Roebber (2009)). A perfect prediction would lie at the top right corner of the performance space, meaning all metrics approach unity, achieving 100% correct predictions. The more we move toward the lower left corner, the more biased are the predictions and the more false positives or misses does a model produce.

The blue and orange circles in the figure show the performance of both models, with the lines depicting the confidence intervals representing the variability in POD and FAR. The POD, FAR, CSI, and bias are calculated by averaging the respective metric values of the test and validation dataset splits of the ensemble model (test and validation performance was very similar). Bootstrapping (not shown) generates the confidence intervals. The mean POD is 0.77 (north) and 0.61 (south), and the SR (1-FAR) is 0.77 and 0.63, respectively. CSI is 0.60 and 0.44, and bias is 0.98 and 0.88.

https://doi.org/10.5194/egusphere-2024-371
Preprint. Discussion started: 23 February 2024

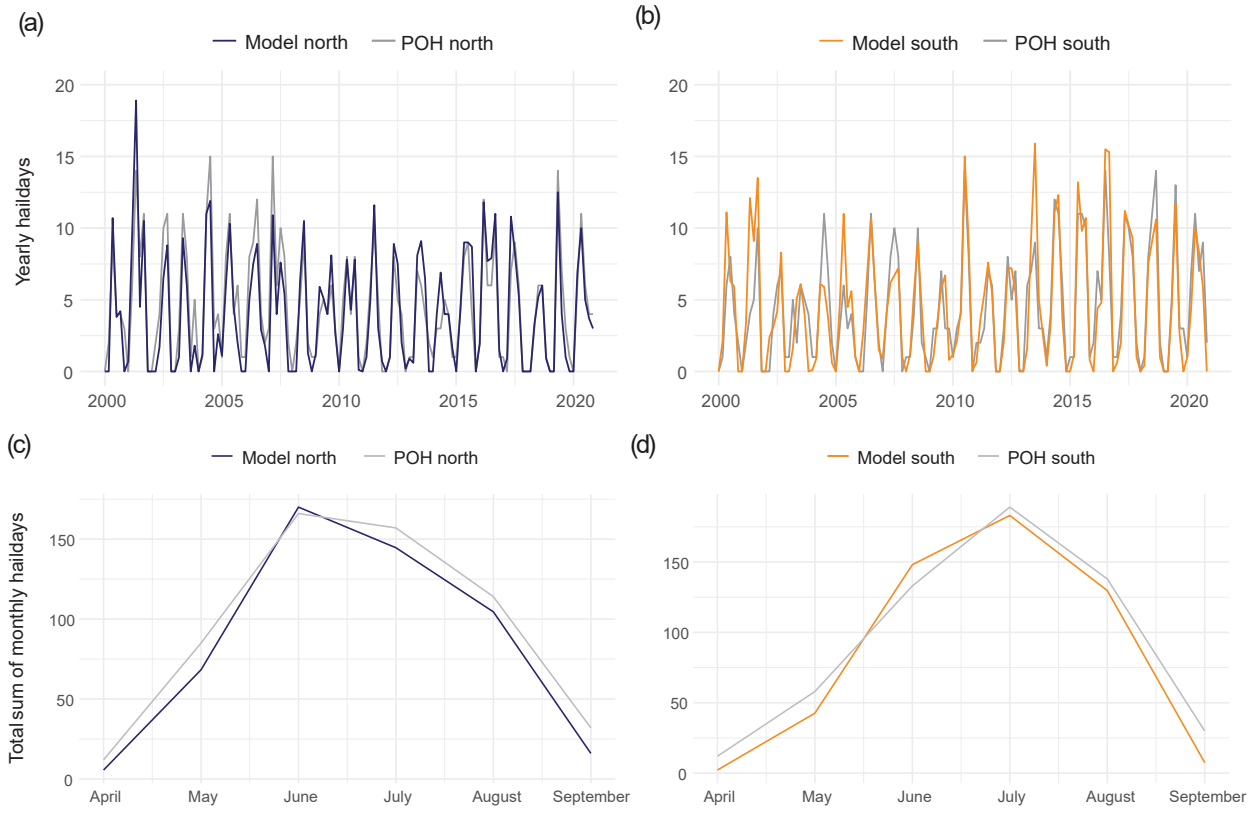

Figure 7. The observed and modelled number of haildays for the period of 2002 - 2012 (April - September) for the northern (a,c) and southern (b,d) domain. Grey lines are the observed number of haildays (POH $\geq$ 80% over min. 580 (north) / 499 (south) km^2). Orange (south) and blue (north) lines are the modelled number of haildays from the ensemble models. Plots (a) and (b) show the absolute number of haildays per year, and (c) and (d) show the sum of haildays per month.

https://doi.org/10.5194/egusphere-2024-371
Preprint. Discussion started: 23 February 2024

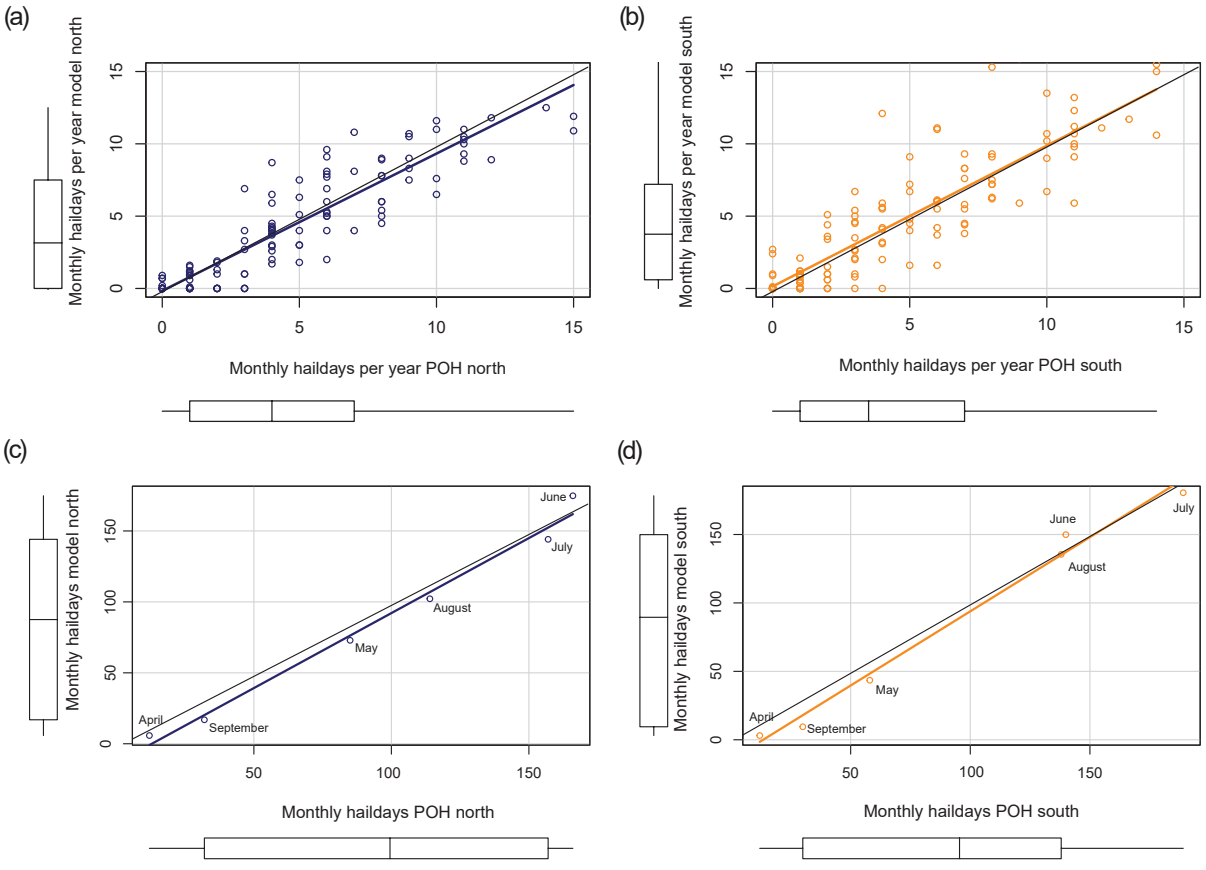

Figure 8. The observed number of haildays (POH $\geq$ 80% over min. 580 (north) / 499 (south) km^2) plotted against the modelled number of haildays from the ensemble models for the northern domain (a,c) and southern domain (b,d) for the whole observational period 2002-2022. Plots (a) and (b) show the absolute number of haildays per year and (c) and (d) show the absolute sum of haildays per month. The black lines are the $x = y$ lines and the orange and blue lines are the fit to the orange and blue circles, respectively. Boxplots show the distribution of the respective samples.

https://doi.org/10.5194/egusphere-2024-371
Preprint. Discussion started: 23 February 2024

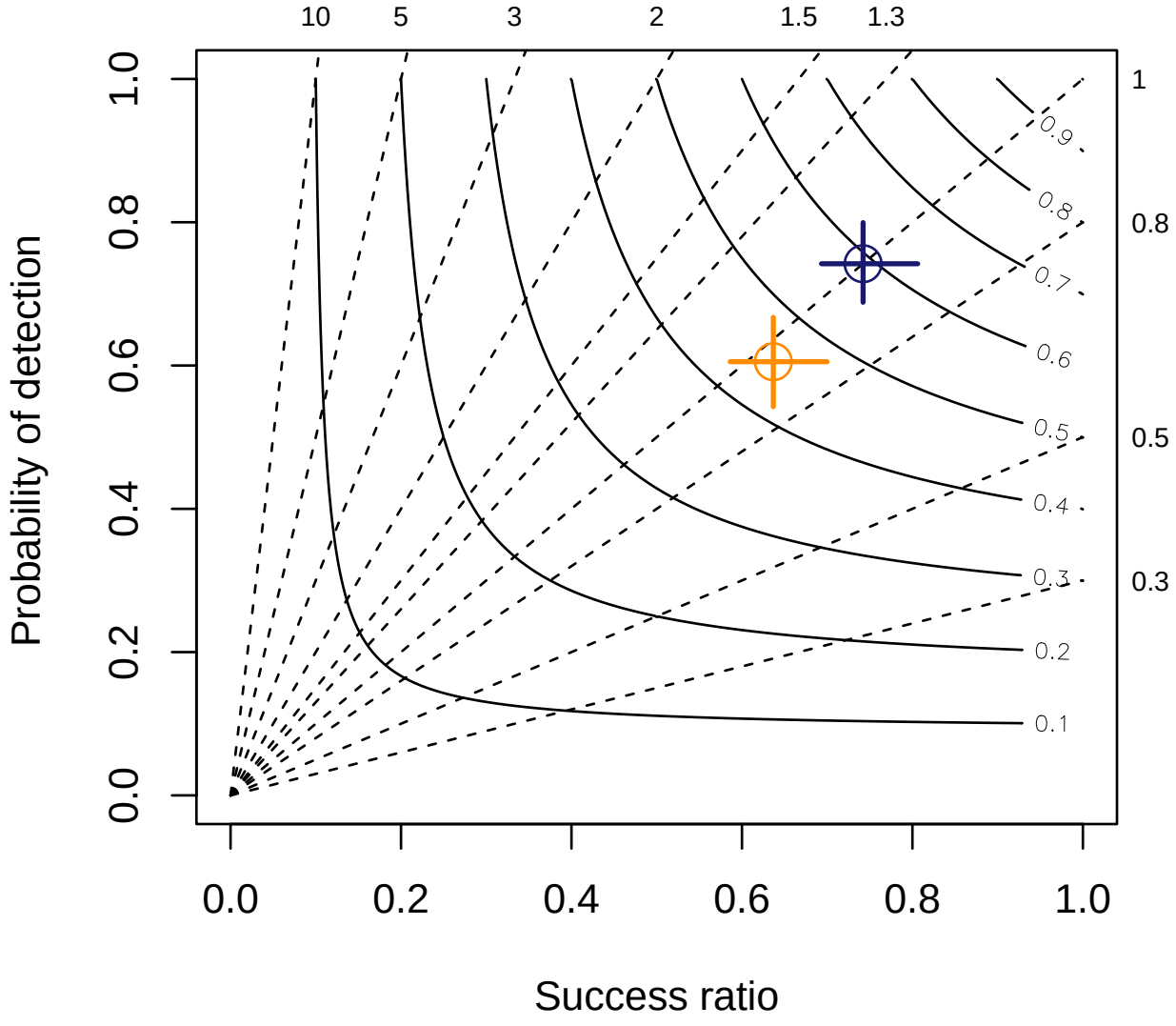

Figure 9. Performance diagram summarizing the POD, SR, bias, and CSI of each model. The orange cross shows the performance skill of the south and the blue cross that of the north. The cross-lines indicate the confidence interval, calculated from bootstrapping. The circles are highlighting the mean value. Dashed lines represent bias scores with labels on the outward extension of the line. Labeled solid contours are CSI.

https://doi.org/10.5194/egusphere-2024-371
Preprint. Discussion started: 23 February 2024

5 Analysis of the reconstructed time series

5.1 Modelled long-term trends

From this section onwards, we will present the reconstructed time series from the ensemble model and discuss its trends, variability, and seasonality.

Figure 10 displays the yearly sum of haildays for the north (left) and the south (right) from 1959 to 2022. We added a linear fit (grey diagonal line with uncertainty range) and performed Mann-Kendall trend tests (or Kendall's tau rank correlation test). τ is 0.355 for the yearly haildays in the north and 0.369 for the south. The p-values are 4.70×10^{-5} and 2.43×10^{-5}respectively. Hence, we have a significant positive trend in yearly hailday occurrence in both regions, which is a bit stronger in the south. The model north estimates a mean of 18.87 haildays per year during the period of 1959 - 2022, with a minimum of 6 in the years 1962 and 1980 and a maximum of 42 in the years 2003 and 2018. In the south, the mean is 20.1, with a minimum of 6 in the year 1984 and a maximum of 41 in the year 2018. In the POH time series, the years 2003 and 2018 are also the years with the (second) highest number of yearly haildays (hailday if POH $\geq$ 80% over min. 580 (north) / 499 (south) km^2) . The mean of yearly haildays for the period 2002 - 2022 is 24.10 (north) and 24.40 (south) for the models, which is slightly lower than that of the POH time series with 24.09 (north) and 25.27 (south) haildays per year. The variability of yearly or monthly sums of haildays increases per decade, with higher variability in the last two decades (not shown).

One might argue that deducing trends from ERA-5 data-driven models can give biased results before 1979, when satellite data were first assimilated in ERA-5. We, therefore, also performed the Mann-Kendall test limited to the period 1979-2022. Tau is 0.318 (north) and 0.463 (south) with a p-value of $1.37 \times e^{-5}$ (north) and $2.87 \times e^{-3}$ (south). This means the trend is still positive and significant in both regions, although a bit less intense in the north and much more pronounced in the south compared to the 1959-2022 period. This discrepancy is caused by the large interannual variability in both time series. The trends for both periods can be compared in Fig. 10 and Fig. 11.

5.2 Drivers of modelled trends

To investigate the factors driving the positive long-term trends in the models, we employed two techniques: partial Mann-Kendall tests and a detrending method proposed by Raupach et al. (2023b)

Using Raupach et al. (2023b) approach, we assess the impact of individual model predictors on hailday trends by applying the models to data in which one of the predictors was detrended by removing the trend in its annual mean. We then performed Mann-Kendall tests to compare how the trend in the whole reconstructed time series from 1959 to 2022 changed. To find which variable has the highest influence on the trend of each model, we compared τ values by changing only one variable at a time with its detrended version for each model. For example, in the southern logistic regression model, detrending the LI resulted in a significant reduction of τ from 0.369 to 0.152, indicating the strong influence of LI on the positive trend. Similarly, detrending only kx, reduced τ to 0.295, while the value only changed marginally with detrending the other predictors. This suggests that the positive trends in annual haildays in the southern logistic model are primarily explained by LI and to a lesser degree by kx , while the other variables like WS_06 contribute marginally. Remember that a direct comparison of τ is possible,

https://doi.org/10.5194/egusphere-2024-371
Preprint. Discussion started: 23 February 2024

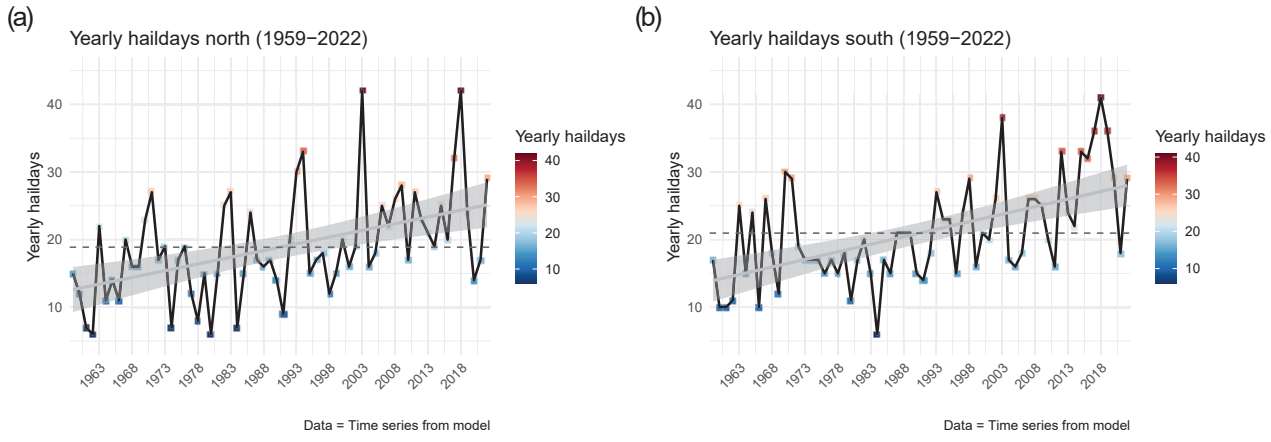

Figure 10. modelled yearly aggregated haildays from 1959 - 2022 (black lines) for the northern (a) and southern (b) domain from the ensemble model. The black dashed lines represent the mean and the grey solid linse plus confidence intervals are the linear fits to the respective yearly haildays from 1959-2022.

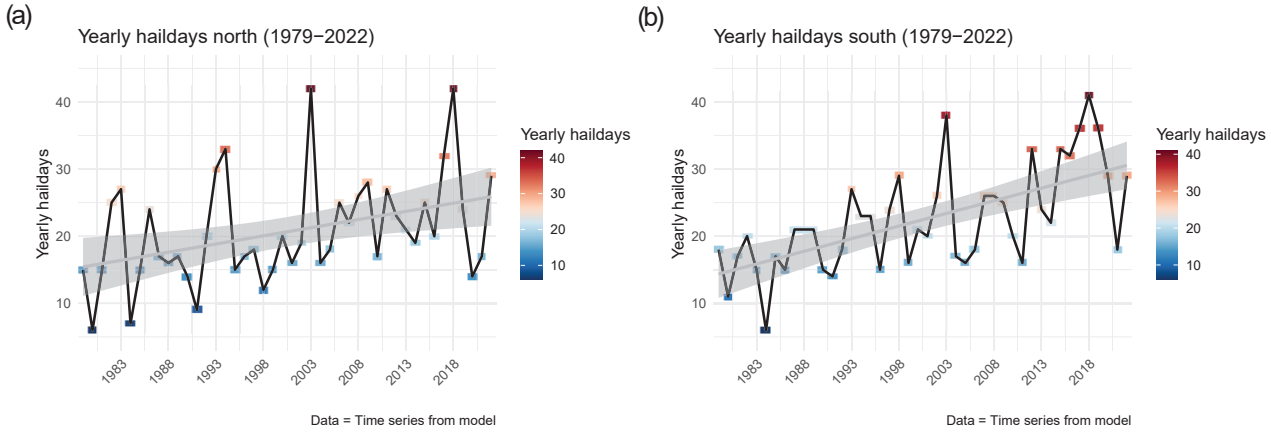

Figure 11. Similar to Fig. 10 but for the period 1979 - 2022. The linear fit is calculated for the yearly haildays from 1979-2022.

as it is independent of the measurement scale. We did this comparison for each model to find which predictors contribute most to the modelled trends. Across all four models (the logistic regression and GAM´s for both domains) the positive trends in annual haildays were primarily driven by instability and moisture variables. To check for the robustness of these results, we also performed partial Mann-Kendall analyses for each model and each model´s predictor. We also performed partial Mann-Kendall tests on the ensemble models with a selection of parameters and saw equal results. The tests showed that, again, in all models, instability and moisture variables are primarily contributing to the trends. It is important to mention that the trend

https://doi.org/10.5194/egusphere-2024-371
Preprint. Discussion started: 23 February 2024

was never fully explained by a single variable but rather by a combination of both moisture and instability. This aligns with the known connection between convective instability and moisture availability.

Figure 12 shows the yearly hailday frequency reconstructed when all model predictors are detrended at the same time. There is a strong natural variability in the yearly hail frequency in both regions. When comparing Fig. 12 with the earlier Fig. 10, we can now graphically see how a decrease in τ translates to a decrease in the slope of the linear trend line.

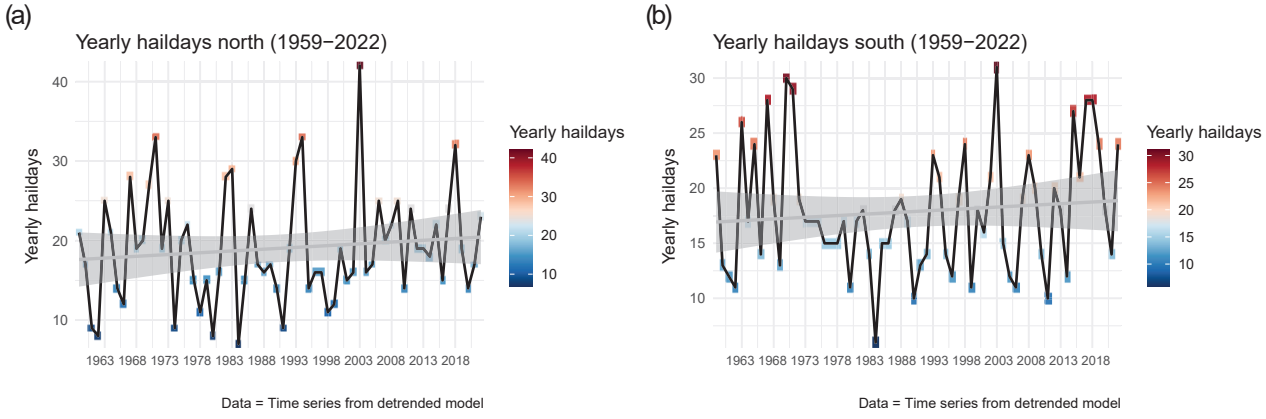

Figure 12. Similar to Fig. 10, but here the yearly aggregated haildays for the northern (a) and southern (b) domain taken from the ensemble model when all predictors are detrended.

Lastly, we need to stress that when we say trend, we are talking about trends in the models only. Of course, the contribution of predictors to the trend depends on the importance of the predictors itself in the models. Additionally, the trend in the model always comes from the underlying trend in the model's predictors. With our analysis, we cannot make assumptions about the "true" trend seen in reality. This will be discussed further in Sect. 6.

5.3 Change in the seasonal cycle over time

This section addresses the seasonal analysis. Boxplots in Fig. 13 (a,b) show the modelled haildays per month for the whole time series period of 1959 - 2022 for both domains. One can see a clear seasonal cycle of hailday occurrence. There is strong year-to-year variability in the monthly number of haildays (see e.g. circles for month July). In Fig. 13 (c,d) the mean number of haildays per month is plotted for each decade in differently colored curves. Decade 1960´s includes the years 1960-1969. The years 1959 and 2020-2022 are excluded, as we wanted to have the same number of years in each decade. In the last two decades (blue and purple curve), there is a strong increase in haildays. This leads to more events specifically at the beginning of the hail season (April-June) and to a shift of the peak of the convective season towards earlier months for both regions. These results are also evident when looking at the seasonal cycle by week or day of the year. Due to the large variability, the differences in the monthly curves are not significant and no systematic shift can be seen (see also cdf plots in Fig. A3). However, as our

https://doi.org/10.5194/egusphere-2024-371
Preprint. Discussion started: 23 February 2024

analysis was limited to the months of April to September, we cannot make assumptions regarding potential changes in hail events in the months preceding or following the modelled period.

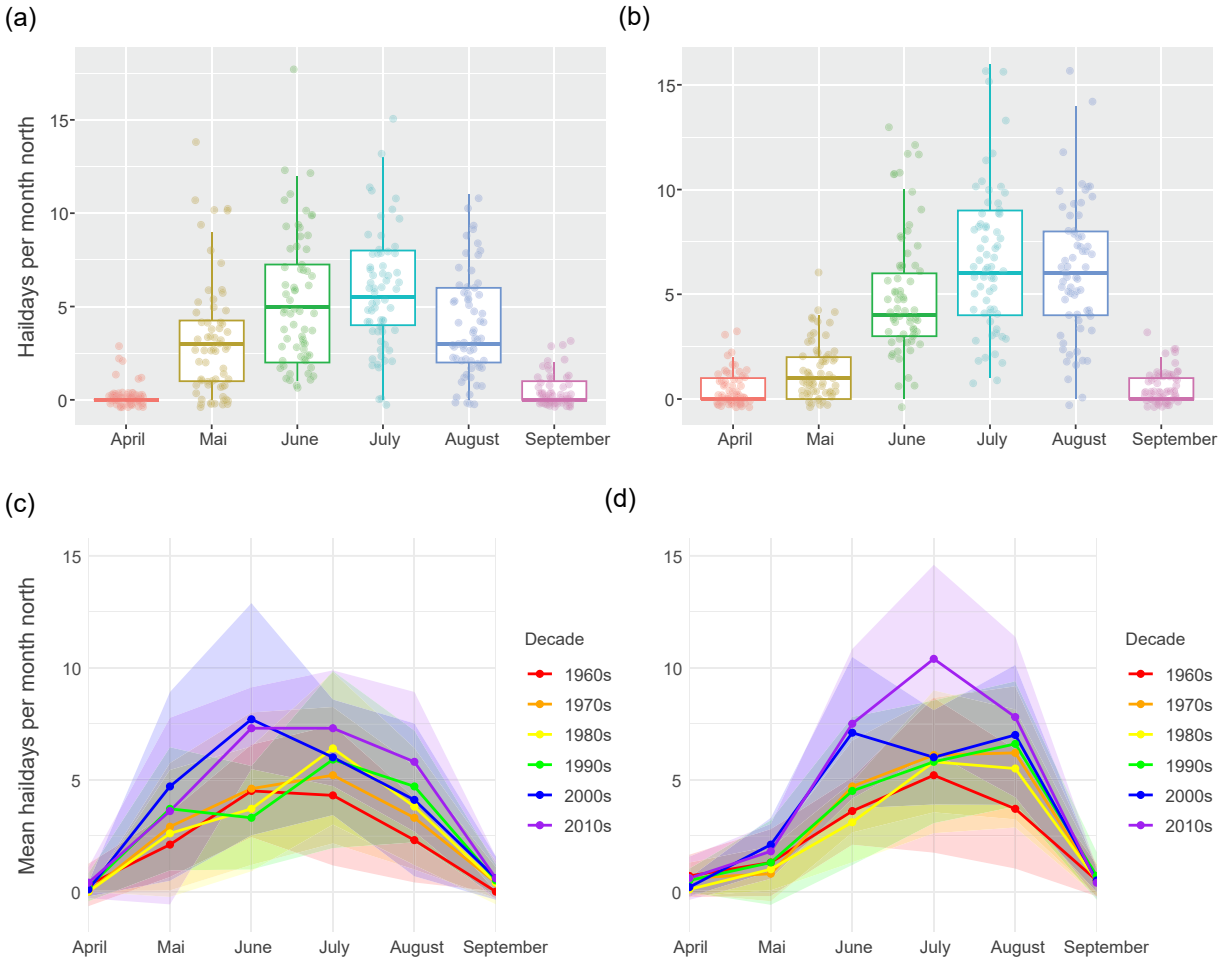

Figure 13. (a) and (b) show boxplots of the modelled number of haildays per month for the whole period 1959-2022. (c) and (d) are the mean number of haildays per month per decade in colored lines plus uncertainty range. Decade 1960´s includes the years 1960-1969 and so on. Plots (a,c) are for the northern domain and (b,d) for the southern domain.

https://doi.org/10.5194/egusphere-2024-371
Preprint. Discussion started: 23 February 2024

5.4 Plausibility check with historic hail data

Validation of our time series and its trends using observational data was not feasible due to the relatively short observational period. Nevertheless, we can conduct plausibility checks with qualitative hail information. As previously mentioned, with this data it is impossible to compare any trends of the modelled time series to that of the historical hail events, as the trends in damages are driven by changes in exposure and vulnerability of crops as well. However, it is possible to compare interannual variability. Figure 14 shows the yearly sum of haildays extracted from the historical hail damage dataset in red from 1959 to 2017. The blue line is the yearly sum of both models. Both time series have been detrended and normalized. The correlation between both time series is 0.43. We did not expect any better results, as even for the period of 2012-2022, where we know, that our model is closer to the true number of hail events than the historical information, some mismatch is evident. When considering the non-detrended and non-normalized yearly time series, both have a similar standard deviation of 5.56 haildays for the model sum and 5.53 for the historic data.

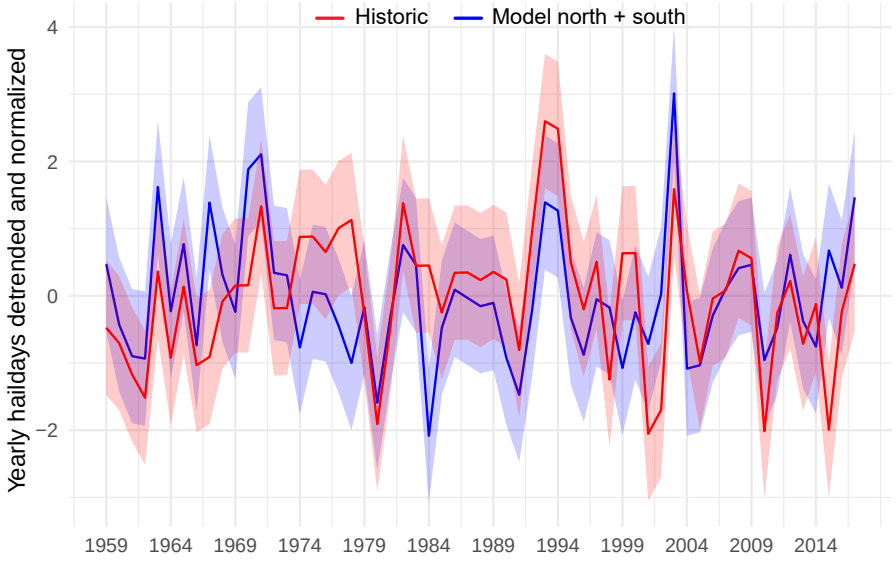

Figure 14. The modelled number of haildays (blue, sum of model north and south) and the number of haildays derived from qualitative agricultural damage data in red (minimum 5 affected municipalities) for the period 1959 - 2017. Both time series have been normalized and detrended.

https://doi.org/10.5194/egusphere-2024-371
Preprint. Discussion started: 23 February 2024

6 Discussion

In this work we evaluated ERA-5 convective parameters and hail occurrence derived from radar data over the years 2012-2022 to develop models reconstructing past haildays in Switzerland. Our analysis has yielded several conclusions, among which the most important ones are discussed below.

6.1 Model predictor selection

Firstly, the predictor selection of the logistic regression models and GAM´s needs to be discussed. Specifically, the absence of wind shear in the logistic regression models of both domains. When training our models, wind shear rarely showed up as a skillful predictor, and if so, then the covariate was not significant in the logistic regression models. This was also the case for the automated feature selection we tested. Our reasoning for this is threefold. Firstly, shear could be indirectly included in the model variable v_500 (v-wind component at 500 hPa; southern model). This variable might have some signal in them while still keeping a linear relationship to the response. We showed earlier that WS_36 (wind shear from 3 - 6km) has a non-linear relationship to the response in the GAM, which the logistic model has difficulty fitting. Moreover, the shear "replacement", as well as the explicit shear variables in the GAM´s, did not have high feature importance. This leads us to our second point, which is that wind shear might be more important for distinguishing between small and large hail (< 2cm) than for the prediction of hail occurrence vs. no hail. Several studies (Brooks et al., 2003; Kaltenböck et al., 2009; Púčik et al., 2015; Taszarek et al., 2020a) have highlighted the importance of wind shear in the formation of hail, as it influences the lifetime and structure of a storm. While large shear values are required to form supercells, which are more likely to produce hail, hail also develops in lower-shear environments (Blair et al., 2021; Kumjian and Lombardo, 2020). Additionally, many of those studies only focussed on large hail (> 2cm or > 5cm). In fact, Markowski and Richardson (2010) and Dennis and Kumjian (2017) showed that wind shear primarily drives storm type and hail diameter. Houze et al. (1993) found that a significant fraction of Swiss hailstorms are not supercells but ordinary and intermediate-type storms. Punge and Kunz (2016) revealed that in complex terrain, high wind shear might not be necessary for hailstorm formation. Hail events in low-shear environments can be explained by a proximity of mountain ranges where environmental wind shear is enhanced by an interaction of the wind field with orography, which is often the case for the Alps (Kunz et al., 2018). Lastly, with such complex terrain, shear might be driven by local conditions (e.g. Alpine pumping) that are too small to be resolved by ERA-5´s resolution. ERA-5 could show weak shear, but due to orographical enhancement, storms actually benefit from larger shear values. This is something that can be better resolved with high-resolution convection permitting models (with approx. 1x1km spatial resolution). We also tried using combinations of shear and CAPE, such as WMAXSHEAR, as seen helpful in studies differentiating between severe and non-severe weather (Brooks et al., 2003; Craven and Brooks, 2004; Kaltenböck et al., 2009; Púčik et al., 2015; Tuovinen et al., 2015), but for both regions, the product did not perform better in combination with other variables.

During model building, we realized that the combination of LI and TT plus other additional information performed very well, and often better than $CAPE$ and shear. This is why three of our models have the combination of LI and TT. However TT can be a problematic parameter for various reasons. Firstly, composite parameters are hard to interpret in a physical

https://doi.org/10.5194/egusphere-2024-371
Preprint. Discussion started: 23 February 2024

context, as they are a combination of multiple information. TT combines two aspects (vertical temperature lapse rates and difference between 850 hPa moisture and 500 hPa temperature) into one number and thus one does not know whether TT is high because the lapse rates are favorable or whether there is plenty of low-level moisture, or a little bit of both. This is also why it is hard to explain why the parameter worked well for our exact problem. In addition, TT takes into account moisture from a fixed single level of 850 hPa, which is very sensitive to rapid changes in dew points with height or spikes, or simply orography. Consequently, TT can be a case-sensitive parameter that may get high values in situations when there is no storm and thus create some false alarms. We think, that the false alarms can be counteracted with the additional information in the model, as it also knows the conditional instability or moisture availability from the additional predictors. We do not claim that the combination of LI and TT are better than e.g. CAPE and shear in differentiating between no hail, hail and large hail. Rather we want to make clear, that our synergy of around five variables in the 5D models worked best for our exact goal and location, namely, reconstructing Swiss haildays in the last 70 years with the POH radar proxy and low-resolution ERA-5 data. We assume that the models learn how to best deal with the limitations of the data sets and chooses the best variables for our specific questions in a data-driven approach. We did not expect to learn about new processes from the models, but the models seem to agree with previous knowledge. We chose ERA-5, as this is the best available product for multidecadal analyses. That said, one should not transfer our models to the future or to other regions around the globe. For forecasting applications the COSMO / ICON 1x1km analyses are much better suited.

The individual 5D models combine information about instability, moisture, shear and other indirect signals in potentially hail favoring environments, but they still suffer from rather high false alarm ratios. With any combination of convective parameters we were not able to increase the explained deviance of the models above approx. 60% for the northern models and 45% for the southern model. This suggests, that there is still some ingredient missing to identify when hail occurs. Notably, the models lack information about convection triggering mechanisms, which can be modified by topography or frontal systems. The Boyden Index (BI, measure for thunderstorm probability associated with frontal passage) is selected in the northern logistic regression model, which showed high feature importance. However, given the equation of the Boyden Index ($= 0.1\,(z_{700} - z_{1000}) - T_{700} - 200$), the authors are cautious as to how much that variable can assess convection triggering. We did test convective inhibition (CIN), but that did not present as skillful predictor. Hence, all models do not include any representation of initiation processes. This "initiation problem" is still a challenge for forecasting thunder- and hailstorms (Lock and Houston, 2014) and causes very high false alarm rates of models in many studies. To battle this problem, one could use convective precipitation as proxy for initiation or produce a model that computes probabilities of hail conditioned on the presence of lightning, e.g. with the AR-CHaMo model, like Battaglioli et al. (2023a) and Rädler et al. (2018) did. Still, even those models show relatively low values of deviance explained (approx. 30%), implying that there is information missing that cannot be captured by conventional convective parameters. This may be a motivation to look further into storm microphysics and e.g. the location of the embryos in time and space during hail favoring environments, instead of relying on instability, shear and moisture parameters.

https://doi.org/10.5194/egusphere-2024-371
Preprint. Discussion started: 23 February 2024

6.2 Comparison to other studies

Several studies have used logistic regression or GAM and daily data to model hail (López et al., 2007; Gascón et al., 2015; Mohr et al., 2015b, a; Rädler et al., 2018; Battaglioli et al., 2023b, a). Often, CAPE and shear are used as main hail model predictors (e.g. Madonna et al. (2018); Battaglioli et al. (2023a); Allen et al. (2015); Czernecki et al. (2019)). As mentioned, in our models, the combination of CAPE and shear only show up in the southern GAM. For the logistic models we found LI to be a better hail predictor than CAPE, which is also mentioned in Mohr et al. (2015b, a) and Rädler et al. (2018). López et al. (2007) use TT (the Total Totals Index) and the wind at 500 hPa as well in their best model for the Iberian Peninsula. Gascón et al. (2015) also used wind at 500 hPa. Unfortunately, we cannot directly compare the coefficients of their model to ours because of differences in data sources, resolution, and combination of model parameters. Those differences must also be considered when comparing our model´s performance to that of other studies. Our ensemble models for the northern and southern domain effectively reproduced the observed year-to-year variability and the seasonal cycle, as depicted in Fig.7 and Fig. 8. While we have not presented a direct comparison between POH and the modelled haildays for the individual logistic regression models and GAMs, all four exhibited very similar characteristics to the ensemble models. This also becomes evident when examining the corresponding performance metrics POD, FAR and CSI across all models. To gauge the predictive capabilities of the models against those in related studies, we will further on use the performance metrics of the ensemble models. Our models outperformed those mentioned in Raupach et al. (2023a) due to lower FAR and higher HSS values. For the different studies, HSS ranges from 0.1 to 0.4 compared to our models' HSS of 0.73 (north) and 0.35 (south). FAR ranges from 0.57 to 0.8 compared to 0.23 (north) and 0.35 (south) for our models. However, there are also studies showing comparable performance skills, like Battaglioli et al. (2023a) using ESWD hail reports and ERA-5 data, López et al. (2007) using radar and radiosonde data and Gascón et al. (2015) using severe storms reports and WRF vertical profiles.

6.3 Trends

Our modelled trends from the ensemble models agree with those seen in Battaglioli et al. (2023a), Madonna et al. (2018), and Rädler et al. (2018). Madonna et al. (2018) found a moderate positive trend in monthly haildays in northern Switzerland from 1979-2014 and Rädler et al. (2018) find an increase of up to 86% in the hail cases per year during the period 1979-2016 in central Europe, Battaglioli et al. (2023a) find a 300% increase in hail hours in northern Italy and parts of southern Switzerland during the period 1950-2022. Albeit not that intense, we also see a strong increase in modelled haildays in the southern domain. This can be attributed to an increase in hail-favoring environments in ERA-5 in recent decades (Taszarek et al., 2021; Pilguj et al., 2022). Many studies find a positive trend in instability and moisture in ERA-5 and rawinsonde data for Europe and parts of Switzerland (Mohr and Kunz, 2013; Pilguj et al., 2022; Taszarek et al., 2021; Rädler et al., 2018, 2019). It is crucial to note, however, that this studies modelled trends in hail occurrence are subject to several limitations. Firstly, POH serves as a proxy, offering an indirect measure of hail, and does not precisely reflect the actual presence of hail on the ground. Additionally, the quality of ERA-5 data has undergone numerous changes over the last decades, introducing various inhomogeneities. The quantity and quality of assimilated observations impact the data quality of ERA-5. Hence, it is

https://doi.org/10.5194/egusphere-2024-371
Preprint. Discussion started: 23 February 2024

not feasible to directly extrapolate our modelled trends into reality. To achieve this, a more extensive period of observational data would be required. However, Pilguj et al. (2022) showed in their study comparing ERA-5 trends to those extracted from rawinsonde data, that the reliability of ERA-5 has increased in the last four decades, meaning we might have higher confidence in the positive trends shown for the period 1979-2022.

Finally, we want to highlight a limitation in the explanation of our trends. Within our models, the positive trend in annual hailday occurrences are driven by moisture and instability predictors (see Sect. 5.1). We can only make assumptions about environmental variables that are selected as predictor in the models. Other factors influencing hail occurence and trends therein, e.g. temperature, could still play an important role, as there is a strong link between temperature, moisture availability and convective instability. Generally, we need to be careful about extrapolating this link outside the observation period, as it might break down in a warmer climate, e.g., with drier summer soils. Studies using CMIP data also showed that over Europe we could see reductions in relative humidity (RH), but increases in the absolute humidity (lower RH, larger dew-points) (Hoogewind et al., 2017; Chen et al., 2020). In the future, despite larger CAPE, the process of convective development may be more difficult due to lower mid-level RH, which leads to a higher lifting condensation level and a higher level of free convection and thus more negative buoyancy and larger CIN (Hoogewind et al., 2017; Chen et al., 2020; Taszarek et al., 2021). Lastly, the rise in the freezing level, induced by lower- to mid-tropospheric warming, could result in hail melting before reaching the ground (Raupach et al., 2023a; Dessens et al., 2015).

7 Conclusion and outlook

In this study, we presented a new multidecadal daily hail time series for northern and southern Switzerland from 1959-2022, reconstructed from a POH radar hail proxy and ERA-5 environmental predictors with the help of statistical models. We built an ensemble model from a multiple logistic regression and a logistic GAM for each domain. Model development steps included the selection of the most hail-relevant predictors based on multiple performance metrics, residual analysis, and multicollinearity, as well as finding the best model settings. The seasonality is explicitly modelled by a categorical factor month in each model. This led to a reduction of systematic biases in the residuals, as well as an improvement in predictive skills. With this time series we wanted to analyse long-term trends and changes in frequency, seasonality and the variability of model-derived Swiss hailstorms in the past decades.

The final ensemble model reproduces the interannual variability and seasonality of the hail proxies well. The reconstructed time series shows a strong significant positive trend in the number of yearly haildays in both regions from 1959-2022. The trend is also significant and positive when looking at the period of 1979-2022. It is mainly driven by instability and moisture predictors in all models. Furthermore, we can see an increase in haildays in April-June in the last two decades and a slightly earlier and longer peak of the hail season compared to earlier decades. Still, there is no clear shift of the whole season towards an earlier start and earlier end, and differences in monthly distributions of all decades are not significant. Lastly, we compared our time series to a historical agricultural insurance data archive. We found overlaps in the weakest and strongest hail years and a similar inter-annual variability, however, only low correlations. The main purpose of this study is to offer an alternative

https://doi.org/10.5194/egusphere-2024-371
Preprint. Discussion started: 23 February 2024

framework to study intra-annual variability, trends, and changes in the seasonality of Swiss hail occurrence in the past without long-term direct hail observations. Our goal was not to predict every hail event in Switzerland per grid cell, but to reconstruct strong haildays in the past. We will use this time series to study local and remote drivers of the intra- and inter-annual variability of Swiss hail. This includes e.g. SST (Cheng et al., 2022; Jeong et al., 2020) and soil moisture anomalies (Taylor, 2015; Gaal and Kinter, 2021) and sea ice and snow cover (Budikova, 2009; Wiese, 1924). Similarly, it would be interesting to see whether the mentioned large-scale variables were related to specific circulation anomalies or synoptic configurations (see e.g. Piper and Kunz (2017); Rohrer et al. (2019); Schemm et al. (2016). This will be subject of future work.

Code and data availability. Radar data is available from MeteoSwiss upon request (https://www.meteoschweiz.admin.ch/ service-und-publikationen/ service.html) with a licensing requirement for commercial use. For access to the Swiss historical hail damage data archive please contact Stefan Müller (stefan.mueller@meteotest.ch). ERA-5 datasets can be downloaded via API request directly from the ECMWF Climate Data Store (CDS, https://cds.climate.copernicus.eu/). For code on model building and diagnostics, please contact Lena Wilhelm (lena.wilhelm@unibe.ch).

https://doi.org/10.5194/egusphere-2024-371
Preprint. Discussion started: 23 February 2024

Appendix A: Further explanations

A1 Model building - GAM smoothing functions

We experimented with different smoothing functions, yet observed only minimal differences in the fitted functions. Since the GAM might be more forgiving to inhomogeneities and non-stationarities, we experimented a lot without the $factor(month)$ and the whole dataset for training the GAM. Nevertheless, the best model was still achieved with both modifications.

A2 Calculation of model performance metrics

AIC (Akaike, 1974) and BIC (Schwarz, 1978) were calculated with the R stats package. The AIC is defined as:

$$AIC = -2 \times ln(L) + k \times n_{par}$$

, where $ln(L)$ is the logarithm of the maximum likelihood of the estimated model, $k = 2$, and n_{par} is the number of fitted model parameters. For glm $-2 \times ln(L)$ is the deviance. Using $k = log(n)$ provides the BIC instead, where n is the number of observations. The VIF was also calculated in R by:

$$VIF_i = 1/(1 - R_i^2)$$

,where R_i^2 is the coefficient of determination obtained when regressing the i^{th} predictor on the others.

https://doi.org/10.5194/egusphere-2024-371
Preprint. Discussion started: 23 February 2024

Appendix A: Figures

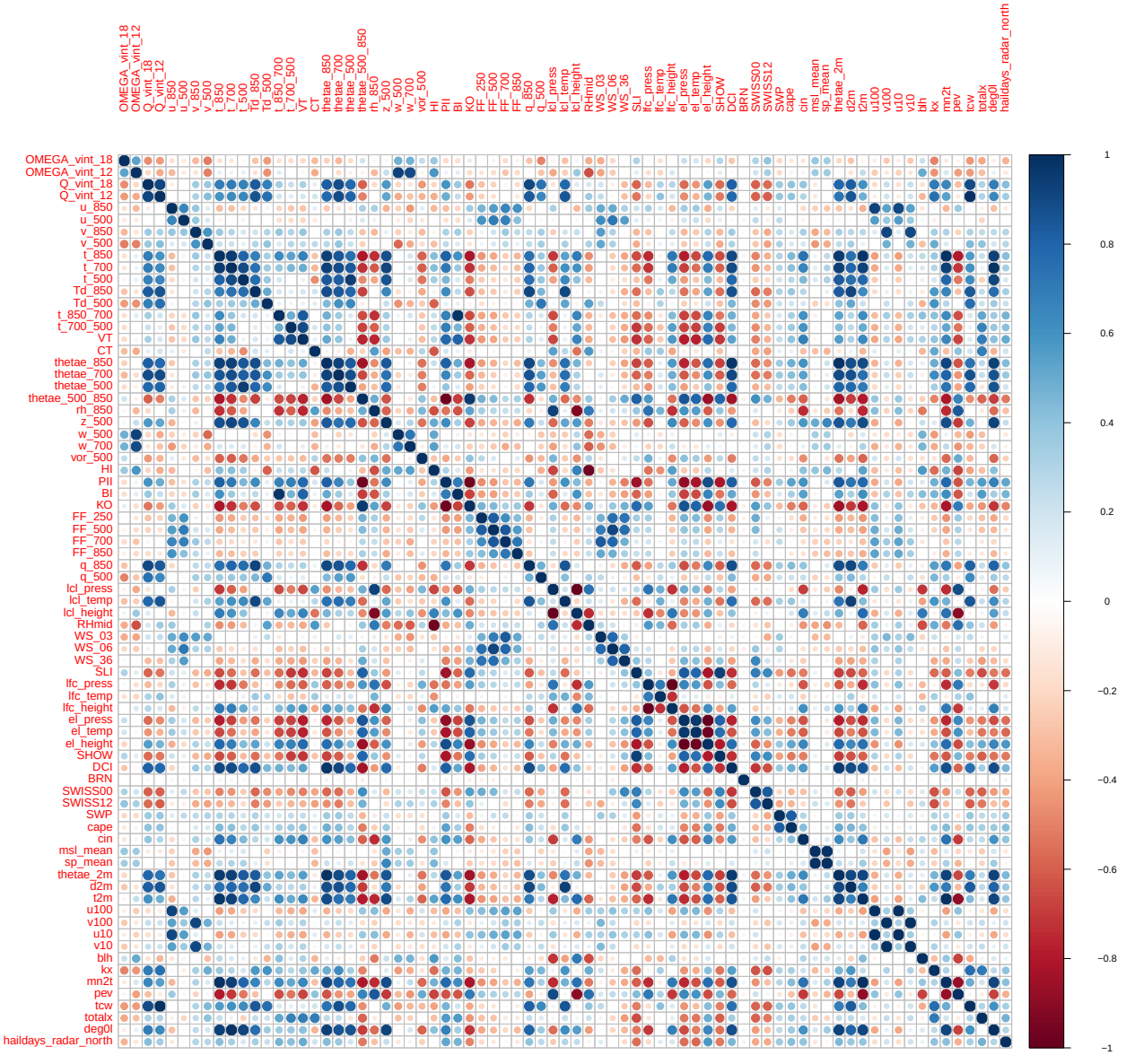

Figure A1. Correlation matrix of all tested model variables and the hailday time series for region north (period 2002-2022).

https://doi.org/10.5194/egusphere-2024-371
Preprint. Discussion started: 23 February 2024

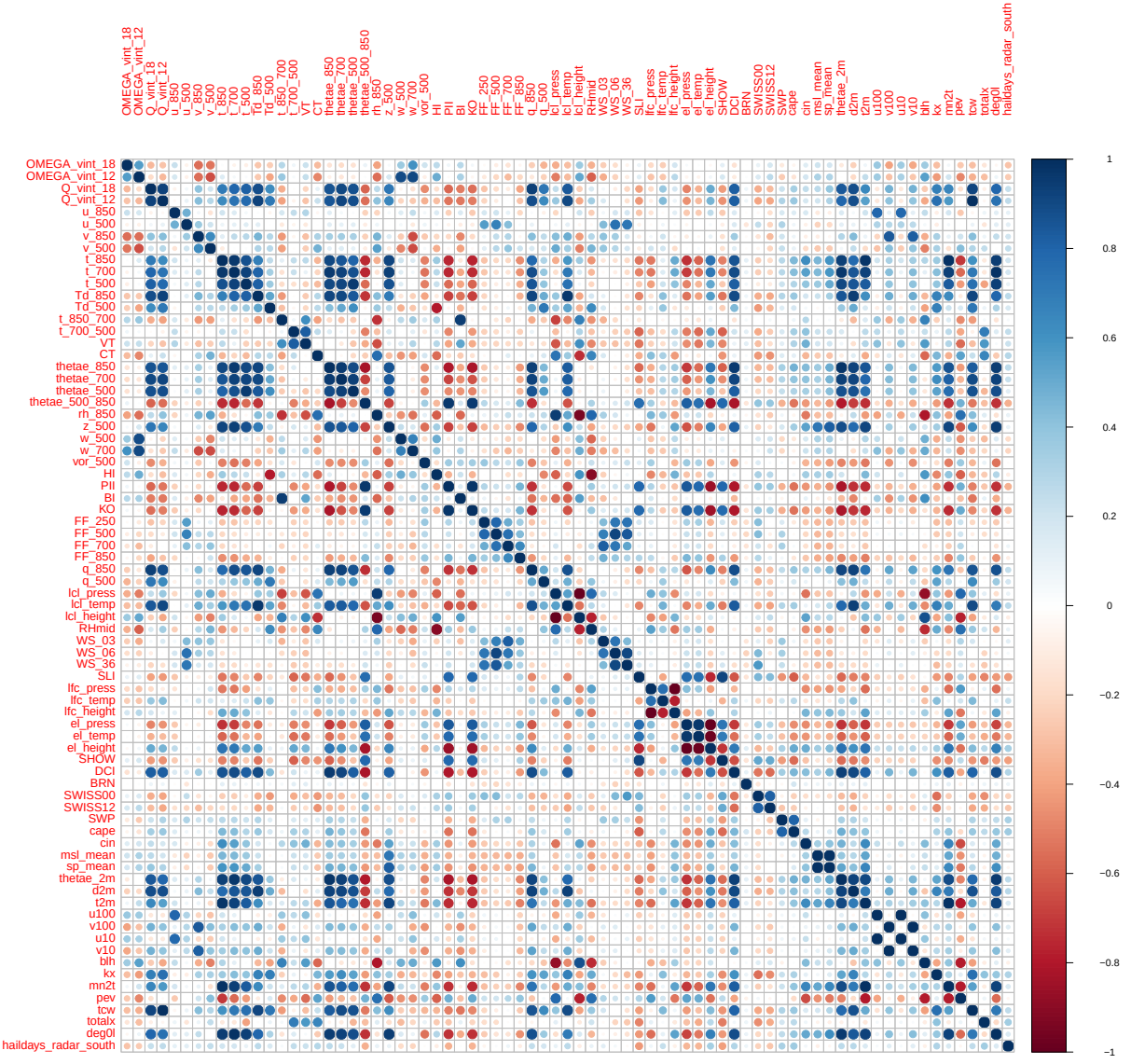

Figure A2. Correlation matrix of all tested model variables and the hailday time series for region south (period 2002-2022).

https://doi.org/10.5194/egusphere-2024-371
Preprint. Discussion started: 23 February 2024

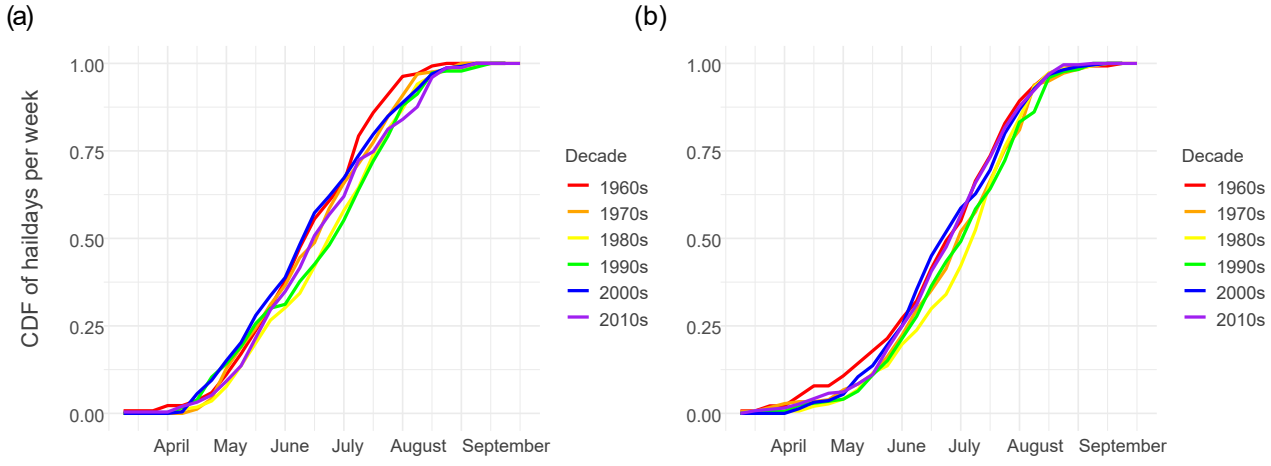

Figure A3. Cumulative distributions functions of the number of haildays per month per decade (colored lines). (a) shows the northern domain and (b) the southern domain.

https://doi.org/10.5194/egusphere-2024-371
Preprint. Discussion started: 23 February 2024

Appendix A: Tables

Table A1. Equations and limits for performance metrics that were used to find the best hail models. Performance metrics were calculated from the respective contingency tables. A are the true positives (TP), B are the false positives (FP), C are the false negatives (FN) and D are the true negatives (TN).

Variable	Explanation	Limits	Perfect Score
POD	$A/(A+C)$	$0 \leq \text{POD} \leq 1$	1
FAR	$B/(A+B)$	$0 \leq \text{FAR} \leq 1$	0
SR	$1-\text{FAR}$	$0 \leq \text{SR} \leq 1$	1
CSI	$A/(A+B+C)$	$0 \leq \text{CSI} \leq 1$	1
HSS	$(2(A \times D - C \times B))/(C^2+B^2+2 \times A \times D+(C+B) \times (A+D))$	$-\infty \leq \text{HSS} \leq 1$	1
Bias	$A+B/(A+C)$	$0 \leq \text{Bias} \leq \infty$	1
Precision	$A/(A+B)$	$0 \leq \text{Precision} \leq 1$	1
Accuracy	$A+D/(A+B+C+D)$	$0 \leq \text{Accuracy} \leq 1$	1

https://doi.org/10.5194/egusphere-2024-371
Preprint. Discussion started: 23 February 2024

Table A2. Summary of convective parameters and meteorological variables tested for model building: T and Td are temperature and dew point temperature, θ_e is equivalent potential temperature, z is the geopotential height (gpdam). The subscript indicates a certain constant pressure level; an arrow indicates lifting of an air parcel (e.g., T′x⟶y is the temperature T of a parcel at the y-level, which was initially lifted dry adiabatically from the x-level to its condensation level and moist adiabatically thereafter)

Variable	Explanation	Unit
BI	Boyden Index $= 0.1\,(z_{700} - z_{1000}) - T_{700} - 200$	Dimensionless
blh	Boundary layer height	m
BRN	Bulk Richardson Number $= \frac{CAPE}{0.5\left(WS\_06^2\right)}$	Dimensionless
CAPE	Most unstable convective available potential energy	J kg^{-1}
cin	Convective inhibition	Jkg^{-1}
CT	Cross Total $= Td_{850} - T_{500}$	K
d2m	Temperature at 2 meters	K
DCI	Deep Convective Index $= T_{850} - Td_{850} - LI$	K
deg0l	Height of zero degree isotherm	m
el_height	Height of equilibrium level	km
el_press	Pressure of equilibrium level	hPa
el_temp	Temperature of equilibrium level	°C
FF_250	Windspeed at 250 hPa	ms^{-1}
FF_500	Windspeed at 500 hPa	ms^{-1}
FF_700	Windspeed at 700 hPa	ms^{-1}
FF_850	Windspeed at 850 hPa	ms^{-1}
HI	Humidity Index $= (T_{850} - Td_{850}) + (T_{700} - Td_{700}) + (T_{500} - Td_{500})$	K
KO	KO Index $= 0.5\,(\theta_{e500} + \theta_{e700}) - 0.5\,(\theta_{e850} + \theta_{e1000})$	K
kx	K Index $= T_{850} + Td_{850} - T_{500} - (T_{700} - Td_{700})$	K
lcl_height	Height of lifted condensation level	km
lcl_press	Pressure of lifted condensation level	hPa
lcl_temp	Temperature of lifted condensation level	K
lfc_height	Height of level of free convection	km
lfc_press	Pressure of level of free convection	hPa
lfc_temp	Temperature of level of free convection	°C
mn2t	Minimum 2 m temperature	K
msl_mean	Mean sea level pressure	Pa
OMEGA_vint	Vertically integrated vertical velocity (model levels 1-137)	Pas^{-1}
OMEGA_vint_18	Vertically integrated vertical velocity at 18 UTC (model levels 1-137)	Pas^{-1}
pev	Potential evaporation	m

Continued on next page

https://doi.org/10.5194/egusphere-2024-371
Preprint. Discussion started: 23 February 2024

Variable	Explanation	Unit
PII	Potential Instability Index $= \frac{\theta_{e925} - \theta_{e500}}{z_{500} - z_{950}}$	Dimensionless
q_500	Specific humidity at 500 hPa	kgkg^{-1}
q_850	Specific humidity at 850 hPa	kgkg^{-1}
Q_vint	Vertically integrated specific humidity (model levels 1-137)	kgkg^{-1}
Q_vint_18	Vertically integrated specific humidity at 18 UTC (model levels 1-137)	kgkg^{-1}
rh_850	Relative Humidity at 850 hPa	%
RHmid	Mean of relative humidity at 500, 700, and 850 hPa	%
SHOW	Showalter Index $= T_{500} - T`_{850 \rightarrow 500}$	K
LI	Surface Based Lifted Index $= T_{500} - T`_{Surface \rightarrow 500}$	K
sp_mean	Mean surface pressure	Pa
SWISS00	Stability and Wind Shear Index for thunderstorms in Switzerland $= SHOW + 0.4\,(WS\_36) + 0.1\,(T_{600} - Td_{600})$	Dimensionless
SWISS12	Stability and Wind Shear Index for thunderstorms in Switzerland $= LI - 0.1\,(WS\_03) + 0.1\,(T_{650} - Td_{650})$	Dimensionless
SWP	Severe Weather Parameter $= CAPE \cdot WS\_06$	Dimensionless
t_500	Temperature at 500 hPa	K
t_700	Temperature at 700 hPa	K
t_700_500	Lapse rate between 700 and 500 hPa	K
t_850	Temperature at 850 hPa	K
t_850_700	Lapse rate between 650 and 700 hPa	K
t2m	Temperature at 2 meters	K
tcw	Total column water from ERA5 single level	kgm^{-2}
Td_500	Temperature at 500 hPa	K
Td_850	Temperature at 850 hPa	K
thetae_2m	Equivalent potential temperature at 2 meters	K
thetae_500	Equivalent potential temperature at 500 hPa	K
thetae_500_850	Difference between equivalent potential temperature at 850 hPa and 500 hPa	K
thetae_700	Equivalent potential temperature at 700 hPa	K
thetae_850	Equivalent potential temperature at 850 hPa	K
totalx	Total Totals Index $= VT + CT$	K
u_500	Zonal wind component at 500 hPa	ms^{-1}
u_850	Zonal wind component at 850 hPa	ms^{-1}

Continued on next page

https://doi.org/10.5194/egusphere-2024-371
Preprint. Discussion started: 23 February 2024

Variable	Explanation	Unit
u10	Zonal wind component at 10 hPa	ms^{-1}
u100	Zonal wind component at 100 hPa	ms^{-1}
v_500	Meridional wind component at 850 hPa	ms^{-1}
v_850	Meridional wind component at 850 hPa	ms^{-1}
v10	Zonal wind component at 10 hPa	ms^{-1}
v100	Meridional wind component at 100 hPa	ms^{-1}
vor_500	Vorticity (relative) at 500 hPa	$1s^{-1}$
VT	Vertical Total $= T_{850} - T_{500}$	K
w_500	Vertical velocity at 500 hPa	Pas^{-1}
w_700	Vertical velocity at 700 hPa	Pas^{-1}
WS_03	Wind shear between 0 km and 3 km	ms^{-1}
WS_06	Wind shear between 0 km and 6 km	ms^{-1}
WS_36	Wind shear between 3 km and 6 km	ms^{-1}
z_500	Geopotential height at 500 hPa	gpdam

End of table

https://doi.org/10.5194/egusphere-2024-371
Preprint. Discussion started: 23 February 2024

Table A3. Mean values, 90^{th} and 10^{th} percentiles of tested model variables of region north and region south separately for the period 1959 to 2022. Mean is the 90^{th} percentile mean.

Variable	Unit	Mean North	90^{th} North	10^{th} North	Mean South	90^{th} South	10^{th} South
BI	Dimensionless	89.61	91.07	87.80	90.00	91.16	88.62
blh	m	1126.11	1463.56	760.87	1133.79	1535.30	718.09
BRN	Dimensionless	0.42	3.56	0.00	0.69	6.00	0.00
CAPE	Jkg^{-1}	15.91	93.54	0.11	26.87	184.18	0.15
cin	Jkg^{-1}	117.67	464.81	1.00	135.36	425.25	5.82
CT	K	20.09	23.48	15.28	19.73	23.13	15.33
d2m	K	282.67	287.62	276.06	281.93	286.99	274.79
DCI	K	10.77	24.41	-5.61	11.30	23.86	-4.47
deg0l	m	2433.65	3426.54	1137.65	2256.94	3161.47	1133.94
el_height	km	4.97	8.93	2.18	6.47	9.51	3.38
el_press	hPa	556.32	777.36	310.24	452.66	667.73	284.47
el_temp	°C	-15.90	0.08	-40.18	-24.20	-3.98	-43.55
FF_250	ms^{-1}	21.11	37.53	8.71	20.33	36.78	7.91
FF_500	ms^{-1}	12.56	22.59	5.04	11.42	21.01	4.39
FF_700	ms^{-1}	7.61	13.60	3.13	5.26	9.70	2.33
FF_850	ms^{-1}	4.98	8.93	2.21	1.92	3.83	0.86
HI	K	26.36	45.83	11.18	47.50	66.37	30.45
KO	K	-0.14	5.99	-6.57	-0.48	4.86	-5.97
kx	K	14.48	25.42	-2.26	16.09	24.10	3.31
lcl_height	km	1.79	2.34	1.33	2.02	2.56	1.54
lcl_press	hPa	816.29	863.71	762.02	793.13	841.12	741.10
lcl_temp	K	278.19	283.30	271.50	277.68	283.16	269.93
lfc_height	km	2.39	4.01	1.49	2.89	4.30	1.93
lfc_press	hPa	758.74	846.97	615.35	712.69	801.57	592.34
lfc_temp	°C	2.09	6.60	-4.99	1.46	6.59	-6.80
mn2t	K	289.53	296.23	282.27	289.26	295.37	281.74
msl_mean	Pa	1016.68	1022.49	1009.82	1015.77	1021.37	1009.04
OMEGA_vint	Pas^{-1}	-84.87	609.52	-1128.85	-165.39	735.05	-1358.83
OMEGA_vint_18	Pas^{-1}	-206.32	614.20	-1406.01	-55.74	811.37	-1244.75
pev	m	-0.00	-0.00	-0.00	-0.00	-0.00	-0.00

Continued on next page

https://doi.org/10.5194/egusphere-2024-371
Preprint. Discussion started: 23 February 2024

Variable	Unit	Mean North	90^{th} North	10^{th} North	Mean South	90^{th} South	10^{th} South
PII	Dimensionless	-0.00	0.02	-0.02	0.00	0.00	-0.00
q_500	$kgkg^{-1}$	0.90	1.65	0.37	0.93	1.68	0.38
q_850	$kgkg^{-1}$	6.40	8.83	4.00	6.72	9.29	3.98
Q_vint	$kgkg^{-1}$	17.44	25.08	10.10	17.17	24.12	9.80
Q_vint_18	$kgkg^{-1}$	18.16	26.15	10.65	17.87	24.99	10.20
rh_850	%	71.46	87.20	49.0	63.54	80.40	45.5
RHmid	%	56.20	76.54	35.97	55.17	74.84	38.84
SHOW	K	0.58	4.88	-3.30	0.06	4.33	-3.49
LI	K	0.15	4.85	-3.85	-0.21	4.37	-3.92
sp_mean	Pa	932.52	937.90	925.57	897.94	903.47	890.87
SWISS00	Dimensionless	7.22	12.77	2.59	8.16	13.29	3.71
SWISS12	Dimensionless	2.87	8.11	-1.38	4.54	8.88	0.56
SWP	Dimensionless	173.59	1039.63	0.87	268.29	1923.29	1.34
t_500	K	257.29	262.21	250.21	257.72	262.61	250.70
t_700	K	273.15	278.60	266.42	273.86	279.04	267.35
t_700_500	K	16.02	18.00	13.82	16.31	18.17	14.30
t_850	K	282.58	289.03	275.48	284.61	289.93	277.80
t_850_700	K	9.65	11.60	7.32	10.85	12.33	9.08
t2m	K	290.58	297.51	282.98	290.21	296.27	282.46
tcw	kgm^{-12}	17.58	25.29	10.22	17.28	24.24	9.90
Td_500	K	245.07	253.18	235.95	245.52	253.33	236.48
Td_850	K	277.00	282.07	270.35	277.27	282.59	270.04
thetae_2m	K	320.92	336.23	304.66	324.27	339.02	307.27
thetae_500	K	316.85	324.03	306.88	317.42	324.50	307.48
thetae_500_850	K	2.30	9.78	-5.24	0.24	7.16	-6.76
thetae_700	K	312.03	321.56	300.80	314.74	324.10	302.90
thetae_850	K	314.32	327.28	300.38	316.99	329.58	302.67
totalx	K	42.41	47.96	34.03	43.37	47.78	37.07
u_500	ms^{-1}	7.33	18.81	-3.58	6.82	17.50	-3.55
u_850	ms^{-1}	1.53	6.40	-2.80	0.14	1.42	-1.46

Continued on next page

https://doi.org/10.5194/egusphere-2024-371
Preprint. Discussion started: 23 February 2024

Variable	Unit	Mean North	90^{th} North	10^{th} North	Mean South	90^{th} South	10^{th} South
u10	ms^{-1}	0.73	2.71	-1.25	-0.03	0.74	-0.82
u100	ms^{-1}	1.01	3.89	-1.76	0.00	1.05	-1.11
v_500	ms^{-1}	0.30	11.44	-10.98	-0.31	10.22	-10.56
v_850	ms^{-1}	0.14	4.30	-3.73	0.76	2.71	-1.45
v10	ms^{-1}	-0.36	1.60	-2.34	0.61	1.39	-0.52
v100	ms^{-1}	-0.46	2.31	-3.23	0.80	1.94	-0.83
vor_500	$1s^{-1}$	-0.00	0.00	-0.00	0.00	0.00	-0.00
VT	K	25.59	29.06	21.85	27.09	29.73	24.26
w_500	Pas^{-1}	-0.02	0.12	-0.22	-0.01	0.15	-0.24
w_700	Pas^{-1}	-0.01	0.13	-0.21	-0.04	0.16	-0.31
WS_03	ms^{-1}	5.92	11.39	2.02	4.76	8.64	1.95
WS_06	ms^{-1}	11.09	20.73	3.85	11.21	20.72	3.99
WS_36	ms^{-1}	6.11	11.66	2.14	7.09	13.63	2.41
z_500	gpdam	559.54	571.90	543.02	560.48	572.61	544.09

End of table

https://doi.org/10.5194/egusphere-2024-371
Preprint. Discussion started: 23 February 2024

Table A4. Correlation of all variables to the hailday time series of both regions. The correlation was only calculated for the period where we have information on haildays, so for years 2002 to 2022. r is the Pearson correlation and p-value is the respective p-value, whereby zero means an extremely small number (smaller than can be calculated by R´s package Hmisc::rcorr).

Variable	r North	p-value North	r South	p-value South
BI	0.03	0.05	-0.00	0.87
blh	0.06	0.00	-0.04	0.01
BRN	0.08	2.24×10^{-6}	0.11	3.16×10^{-12}
CAPE	0.49	0.00	0.45	0.00
cin	0.40	0.00	0.06	0.01
CT	0.22	0.00	0.29	0.00
d2m	0.39	0.00	0.34	0.00
DCI	0.44	0.00	0.36	0.00
deg0l	0.28	0.00	0.23	0.00
el_height	0.56	0.00	0.39	0.00
el_press	-0.53	0.00	-0.38	0.00
el_temp	-0.56	0.00	-0.39	0.00
FF_250	-0.13	2.22×10^{-16}	-0.06	0.00
FF_500	-0.09	6.98×10^{-8}	-0.00	0.86
FF_700	0.01	0.60	0.03	0.04
FF_850	-0.07	1.08×10^{-5}	-0.07	5.97×10^{-6}
HI	-0.07	4.65×10^{-5}	-0.06	9.42×10^{-5}
KO	-0.49	0.00	-0.42	0.00
kx	0.39	0.00	0.33	0.00
lcl_height	0.12	1.31×10^{-13}	-0.11	1.35×10^{-11}
lcl_press	-0.12	4.48×10^{-13}	0.10	3.35×10^{-10}
lcl_temp	0.34	0.00	0.33	0.00
lfc_height	0.18	0.00	-0.02	0.35
lfc_press	-0.20	0.00	0.00	0.86
lfc_temp	0.15	0.00	0.23	0.00
mn2t	0.40	0.00	0.26	0.00
msl_mean	-0.13	4.44×10^{-16}	-0.09	2.06×10^{-8}
OMEGA_vint	-0.19	0.00	-0.26	0.00
OMEGA_vint_18	-0.31	0.00	-0.26	0.00
pev	-0.29	0.00	-0.10	1.36×10^{-9}

Continued on next page

https://doi.org/10.5194/egusphere-2024-371
Preprint. Discussion started: 23 February 2024

Variable	r North	p-value North	r South	p-value South
PII	0.52	0.00	-0.42	0.00
q_500	0.26	0.00	0.20	0.00
q_850	0.42	0.00	0.33	0.00
Q_vint_12	0.40	0.00	0.33	0.00
Q_vint_18	0.44	0.00	0.32	0.00
rh_850	-0.06	0.00	0.03	0.07
RHmid	0.01	0.70	0.03	0.06
SHOW	-0.46	0.00	-0.40	0.00
LI	-0.47	0.00	-0.41	0.00
sp_mean	-0.06	0.00	-0.02	0.14
SWISS00	-0.38	0.00	-0.27	0.00
SWISS12	-0.37	0.00	-0.30	0.00
SWP	0.43	0.00	0.41	0.00
t_500	0.20	0.00	0.17	0.00
t_700	0.31	0.00	0.26	0.00
t_700_500	0.30	0.00	0.25	0.00
t_850	0.41	0.00	0.28	0.00
t_850_700	0.39	0.00	0.11	7.93×10^{-12}
t2m	0.38	0.00	0.25	0.00
tcw	0.39	0.00	0.33	0.00
Td_500	0.22	0.00	0.19	0.00
Td_850	0.36	0.00	0.33	0.00
thetae_2m	0.45	0.00	0.35	0.00
thetae_500	0.23	0.00	0.19	0.00
thetae_500_850	-0.51	0.00	-0.42	0.00
thetae_700	0.39	0.00	0.30	0.00
thetae_850	0.44	0.00	0.35	0.00
totalx	0.35	0.00	0.30	0.00
u_500	0.04	0.01	0.12	1.78×10^{-14}
u_850	0.01	0.47	0.08	1.33×10^{-7}

Continued on next page

https://doi.org/10.5194/egusphere-2024-371
Preprint. Discussion started: 23 February 2024

Variable	r North	p-value North	r South	p-value South
u10	-0.02	0.34	0.05	0.00
u100	-0.02	0.28	0.05	0.00
v_500	0.29	0.00	0.22	0.00
v_850	0.23	0.00	0.16	0.00
v10	0.17	0.00	0.10	3.40×10^{-10}
v100	0.17	0.00	0.10	2.10×10^{-10}
vor_500	-0.13	2.00×10^{-15}	0.04	0.01
VT	0.42	0.00	0.24	0.00
w_500	-0.16	0.00	-0.20	0.00
w_700	-0.13	1.33×10^{-15}	-0.21	0.00
WS_03	0.14	0.00	0.07	3.41×10^{-5}
WS_06	0.00	0.76	0.01	0.55
WS_36	-0.15	0.00	-0.04	0.02
z_500	0.19	0.00	0.14	0.00

End of table

Author contributions. LW: Conceptualization, data curation, methodology, visualization, writing - original draft and review & editing. OM, CS, and KS: Supervision, conceptualization, methodology, writing - review & editing. MT: Helpful discussions and writing - review & editing.

Competing interests. The contact author has declared that neither they nor their co-authors have any conflict of interest.

Acknowledgements. Firstly we like to thank MeteoSwiss for providing POH data and Mateusz Taszarek for providing the convective parameter dataset from ThundeR to test additional parameters for possible improvements of the models. We also like to thank Stefan Müller for the provision and helpful insights into the historical hail data archive. Thank you to Hélène Barras for her insights into her POH thresholds. Finally, we thank all scClim (https://scclim.ethz.ch/) researchers for valuable inputs throughout the project. This study was funded by the Swiss National Science Foundation (SNF) Grant CRSII5_201792.

https://doi.org/10.5194/egusphere-2024-371
Preprint. Discussion started: 23 February 2024

Appendix: References

Akaike, H.: A new look at the statistical model identification, IEEE Transactions on Automatic Control, 19, 716–723, https://doi.org/10.1109/TAC.1974.1100705, 1974.

Allen, J., Karoly, D., and Mills, G.: A severe thunderstorm climatology for Australia and associated thunderstorm environments, Australian Meteorological and Oceanographic Journal, 61, 143–158, https://doi.org/10.22499/2.6103.001, 2011.

Allen, J. T., Tippett, M. K., and Sobel, A. H.: An empirical model relating U.S. monthly hail occurrence to large-scale meteorological environment, Journal of Advances in Modeling Earth Systems, 7, 226–243, https://doi.org/10.1002/2014MS000397, 2015.

Allen, J. T., Giammanco, I. M., Kumjian, M. R., Jurgen Punge, H., Zhang, Q., Groenemeijer, P., Kunz, M., and Ortega, K.: Understanding Hail in the Earth System, Reviews of Geophysics, 58, https://doi.org/10.1029/2019RG000665, 2020.

Andersson, T., Andersson, M., Jacobsson, C., and Nilsson, S.: Thermodynamic indices for forecasting thunderstorms in southern Sweden, Meteor. Mag., pp. 141–146, 1989.

Applequist, S., Gahrs, G. E., Pfeffer, R. L., and Niu, X.-F.: Comparison of Methodologies for Probabilistic Quantitative Precipitation Forecasting*, Weather and Forecasting, 17, 783–799, https://doi.org/10.1175/1520-0434(2002)017<0783:COMFPQ>2.0.CO;2, 2002.

Augenstein, M., Mohr, S., and Kunz, M.: Trends of thunderstorm activity and relation to large-scale atmospheric conditions in western and central Europe, other, display, https://doi.org/10.5194/ecss2023-98, 2023.

BAFU: Umgang mit Naturgefahren in der Schweiz - Bericht des Bundesrats in Erfuellung des Postulats 12.4271 Darbellay vom 14.12.2012, Technischer Bericht, Bundesamt fuer Umwelt (BAFU), 2012.

Baldauf, M., Seifert, A., Förstner, J., Majewski, D., Raschendorfer, M., and Reinhardt, T.: Operational Convective-Scale Numerical Weather Prediction with the COSMO Model: Description and Sensitivities, Monthly Weather Review, 139, 3887–3905, https://doi.org/10.1175/MWR-D-10-05013.1, 2011.

Barras, H., Martius, O., Nisi, L., Schroeer, K., Hering, A., and Germann, U.: Multi-day hail clusters and isolated hail days in Switzerland – large-scale flow conditions and precursors, Weather and Climate Dynamics, 2, 1167–1185, https://doi.org/10.5194/wcd-2-1167-2021, 2021.

Battaglioli, F., Groenemeijer, P., Púčik, T., Taszarek, M., Ulbrich, U., and Rust, H.: Modelled multidecadal trends of lightning and (very) large hail in Europe and North America (1950–2021), Journal of Applied Meteorology and Climatology, https://doi.org/10.1175/JAMC-D-22-0195.1, 2023a.

Battaglioli, F., Groenemeijer, P., Tsonevsky, I., and Púčik, T.: Forecasting Large Hail and Lightning using Additive Logistic Regression Models and the ECMWF Reforecasts, preprint, Atmospheric, Meteorological and Climatological Hazards, https://doi.org/10.5194/nhess-2023-40, 2023b.

Billet, J., DeLisi, M., Smith, B. G., and Gates, C.: Use of Regression Techniques to Predict Hail Size and the Probability of Large Hail, Weather and Forecasting, 12, 154–164, https://doi.org/10.1175/1520-0434(1997)012<0154:UORTTP>2.0.CO;2, 1997.

Blair, S. F., Deroche, D. R., Boustead, J. M., Leighton, J. W., Barjenbruch, B. L., and Gargan, W. P.: Radar-Based Assessment of the Detectability of Giant Hail, E-Journal of Severe Storms Meteorology, 6, 1–30, https://doi.org/10.55599/ejssm.v6i7.34, 2021.

Boyden, C. J.: A simple instability index for use as a synoptic parameter, Meteor. Mag., pp. 198–210, 1963.

Brooks, H. E., Lee, J. W., and Craven, J. P.: The spatial distribution of severe thunderstorm and tornado environments from global reanalysis data, Atmospheric Research, 67-68, 73–94, https://doi.org/10.1016/S0169-8095(03)00045-0, 2003.

https://doi.org/10.5194/egusphere-2024-371
Preprint. Discussion started: 23 February 2024

Brooks, H. E., Anderson, A. R., Riemann, K., Ebbers, I., and Flachs, H.: Climatological aspects of convective parameters from the NCAR-/NCEP reanalysis, Atmospheric Research, 83, 294–305, https://doi.org/10.1016/j.atmosres.2005.08.005, 2007.

Budikova, D.: Role of Arctic sea ice in global atmospheric circulation: A review, Global and Planetary Change, 68, 149–163, https://doi.org/10.1016/j.gloplacha.2009.04.001, 2009.

Cacciamani, C., Battaglia, F., Patruno, P., Pomi, L., Selvini, A., and Tibaldi, S.: A climatological study of thunderstorm activity in the Po Valley, Theoretical and Applied Climatology, 50, 185–203, https://doi.org/10.1007/BF00866116, 1995.

Chen, J., Dai, A., Zhang, Y., and Rasmussen, K. L.: Changes in Convective Available Potential Energy and Convective Inhibition under Global Warming, Journal of Climate, 33, 2025–2050, https://doi.org/10.1175/JCLI-D-19-0461.1, 2020.

Cheng, K., Harris, L., Bretherton, C., Merlis, T. M., Bolot, M., Zhou, L., Kaltenbaugh, A., Clark, S., and Fueglistaler, S.: Impact of Warmer Sea Surface Temperature on the Global Pattern of Intense Convection: Insights From a Global Storm Resolving Model, Geophysical Research Letters, 49, e2022GL099 796, https://doi.org/10.1029/2022GL099796, 2022.

Costa, S., Mezzasalma, P., Levizzani, V., Alberoni, P., and Nanni, S.: Deep convection over Northern Italy: synoptic and thermodynamic analysis, Atmospheric Research, 56, 73–88, https://doi.org/10.1016/S0169-8095(00)00091-0, 2001.

Craven, J. P. and Brooks, H.: Baseline climatology of sounding derived parameters associated with deep moist convection, Natl. Weather Dig., 28, 13–24, 2004.

Czernecki, B., Taszarek, M., Marosz, M., Półrolniczak, M., Kolendowicz, L., Wyszogrodzki, A., and Szturc, J.: Application of machine learning to large hail prediction - The importance of radar reflectivity, lightning occurrence and convective parameters derived from ERA5, Atmospheric Research, 227, 249–262, https://doi.org/10.1016/j.atmosres.2019.05.010, 2019.

Davison, A. and Huser, R.: Statistics of Extremes, Annual Review of Statistics and Its Application, 2, 203–235, https://doi.org/10.1146/annurev-statistics-010814-020133, 2015.

Dennis, E. J. and Kumjian, M. R.: The Impact of Vertical Wind Shear on Hail Growth in Simulated Supercells, Journal of the Atmospheric Sciences, 74, 641–663, https://doi.org/10.1175/JAS-D-16-0066.1, 2017.

Dessens, J., Berthet, C., and Sanchez, J.: Change in hailstone size distributions with an increase in the melting level height, Atmospheric Research, 158-159, 245–253, https://doi.org/10.1016/j.atmosres.2014.07.004, 2015.

Feldmann, M., Germann, U., Gabella, M., and Berne, A.: A Characterisation of Alpine Mesocyclone Occurrence, preprint, Other aspects of weather and climate dynamics, https://doi.org/10.5194/wcd-2021-53, 2021.

Foote, B., Krauss, T. W., and Makitov, V.: Hail metrics using conventional radar, in: Proceedings of the 16th Conference on Planned and Inadvertent Weather Modification, https://ams.confex.com/ams/Annual2005/techprogram/paper_86773.htm, 2005.

Gaal, R. and Kinter, J. L.: Soil Moisture Influence on the Incidence of Summer Mesoscale Convective Systems in the U.S. Great Plains, Monthly Weather Review, 149, 3981–3994, https://doi.org/10.1175/MWR-D-21-0140.1, 2021.

Galway, J. G.: The Lifted Index as a Predictor of Latent Instability, Bulletin of the American Meteorological Society, 37, 528–529, https://doi.org/10.1175/1520-0477-37.10.528, 1956.

García-Ortega, E., Merino, A., López, L., and Sánchez, J.: Role of mesoscale factors at the onset of deep convection on hailstorm days and their relation to the synoptic patterns, Atmospheric Research, 114-115, 91–106, https://doi.org/10.1016/j.atmosres.2012.05.017, 2012.

Gascón, E., Merino, A., Sánchez, J., Fernández-González, S., García-Ortega, E., López, L., and Hermida, L.: Spatial distribution of thermodynamic conditions of severe storms in southwestern Europe, Atmospheric Research, 164-165, 194–209, https://doi.org/10.1016/j.atmosres.2015.05.012, 2015.

https://doi.org/10.5194/egusphere-2024-371
Preprint. Discussion started: 23 February 2024

Gensini, V. A., Converse, C., Ashley, W. S., and Taszarek, M.: Machine learning classification of significant tornadoes and hail in the U.S. using ERA5 proximity soundings, Weather and Forecasting, https://doi.org/10.1175/WAF-D-21-0056.1, 2021.

George, J.: Weather forecasting for aeronautics., Quarterly Journal of the Royal Meteorological Society, 87, 120–120, https://doi.org/10.1002/qj.49708737120, 1961.

Giaiotti, D., Nordio, S., and Stel, F.: The climatology of hail in the plain of Friuli Venezia Giulia, Atmospheric Research, 67-68, 247–259, https://doi.org/10.1016/S0169-8095(03)00084-X, 2003.

Greene, D. R. and Clark, R. A.: Vertically Integrated Liquid Water—A New Analysis Tool, Monthly Weather Review, 100, 548–552, https://doi.org/10.1175/1520-0493(1972)100<0548:VILWNA>2.3.CO;2, 1972.

Groenemeijer, P. and van Delden, A.: Sounding-derived parameters associated with large hail and tornadoes in the Netherlands, Atmospheric Research, 83, 473–487, https://doi.org/10.1016/j.atmosres.2005.08.006, 2007.

Hastie, T. and Tibshirani, R.: Generalized Additive Models: Some Applications, Journal of the American Statistical Association, 82, 371–386, https://doi.org/10.1080/01621459.1987.10478440, 1987.

Hersbach, H., Bell, B., Berrisford, P., Hirahara, S., Horányi, A., Muñoz-Sabater, J., Nicolas, J., Peubey, C., Radu, R., Schepers, D., Simmons, A., Soci, C., Abdalla, S., Abellan, X., Balsamo, G., Bechtold, P., Biavati, G., Bidlot, J., Bonavita, M., De Chiara, G., Dahlgren, P., Dee, D., Diamantakis, M., Dragani, R., Flemming, J., Forbes, R., Fuentes, M., Geer, A., Haimberger, L., Healy, S., Hogan, R. J., Hólm, E., Janisková, M., Keeley, S., Laloyaux, P., Lopez, P., Lupu, C., Radnoti, G., De Rosnay, P., Rozum, I., Vamborg, F., Villaume, S., and Thépaut, J.: The ERA5 global reanalysis, Quarterly Journal of the Royal Meteorological Society, 146, 1999–2049, https://doi.org/10.1002/qj.3803, 2020.

Hitchens, N. M., Brooks, H. E., and Kay, M. P.: Objective Limits on Forecasting Skill of Rare Events, Weather and Forecasting, 28, 525–534, https://doi.org/10.1175/WAF-D-12-00113.1, 2013.

Hoogewind, K. A., Baldwin, M. E., and Trapp, R. J.: The Impact of Climate Change on Hazardous Convective Weather in the United States: Insight from High-Resolution Dynamical Downscaling, Journal of Climate, 30, 10 081–10 100, https://doi.org/10.1175/JCLI-D-16-0885.1, 2017.

Hosmer, D. W. and Lemeshow, S.: Applied Logistic Regression, Wiley, 1 edn., https://doi.org/10.1002/0471722146, 2000.

Houze, R. A., Schmid, W., Fovell, R. G., and Schiesser, H.-H.: Hailstorms in Switzerland: Left Movers, Right Movers, and False Hooks, Monthly Weather Review, 121, 3345–3370, https://doi.org/10.1175/1520-0493(1993)121<3345:HISLMR>2.0.CO;2, 1993.

Huntrieser, H., Schiesser, H. H., Schmid, W., and Waldvogel, A.: Comparison of Traditional and Newly Developed Thunderstorm Indices for Switzerland, Weather and Forecasting, 12, 108–125, https://doi.org/10.1175/1520-0434(1997)012<0108:COTAND>2.0.CO;2, 1997.

Jeong, J.-H., Fan, J., Homeyer, C. R., and Hou, Z.: Understanding Hailstone Temporal Variability and Contributing Factors over the U.S. Southern Great Plains, Journal of Climate, 33, 3947–3966, https://doi.org/10.1175/JCLI-D-19-0606.1, 2020.

Johns, R. H. and Doswell, C. A.: Severe Local Storms Forecasting, Weather and Forecasting, 7, 588–612, https://doi.org/10.1175/1520-0434(1992)007<0588:SLSF>2.0.CO;2, 1992.

Johnson, A. W. and Sugden, K. E.: Evaluation of Sounding-Derived Thermodynamic and Wind-Related Parameters Associated with Large Hail Events, E-Journal of Severe Storms Meteorology, 9, 1–42, https://doi.org/10.55599/ejssm.v9i5.57, 2021.

Kaltenboeck, R. and Steinheimer, M.: Radar-based severe storm climatology for Austrian complex orography related to vertical wind shear and atmospheric instability, Atmospheric Research, 158-159, 216–230, https://doi.org/10.1016/j.atmosres.2014.08.006, 2015.

Kaltenböck, R., Diendorfer, G., and Dotzek, N.: Evaluation of thunderstorm indices from ECMWF analyses, lightning data and severe storm reports, Atmospheric Research, 93, 381–396, https://doi.org/10.1016/j.atmosres.2008.11.005, 2009.

https://doi.org/10.5194/egusphere-2024-371
Preprint. Discussion started: 23 February 2024

Katz, R. W. and Garcia, R. R.: Statistical relationships between hailfall and damage to wheat, Agricultural Meteorology, 24, 29–43, https://doi.org/10.1016/0002-1571(81)90031-5, 1981.

Kopp, J., Schröer, K., Schwierz, C., Hering, A., Germann, U., and Martius, O.: The summer 2021 Switzerland hailstorms: weather situation, major impacts and unique observational data, Weather, 78, 184–191, https://doi.org/10.1002/wea.4306, 2023.

Kumjian, M. R. and Lombardo, K.: A Hail Growth Trajectory Model for Exploring the Environmental Controls on Hail Size: Model Physics and Idealized Tests, Journal of the Atmospheric Sciences, 77, 2765–2791, https://doi.org/10.1175/JAS-D-20-0016.1, 2020.

Kumjian, M. R., Lombardo, K., and Loeffler, S.: The Evolution of Hail Production in Simulated Supercell Storms, Journal of the Atmospheric Sciences, https://doi.org/10.1175/JAS-D-21-0034.1, 2021.

Kunz, M.: The skill of convective parameters and indices to predict isolated and severe thunderstorms, Natural Hazards and Earth System Sciences, 7, 327–342, https://doi.org/10.5194/nhess-7-327-2007, 2007.

Kunz, M. and Puskeiler, M.: High-resolution assessment of the hail hazard over complex terrain from radar and insurance data, Meteorologische Zeitschrift, 19, 427–439, https://doi.org/10.1127/0941-2948/2010/0452, 2010.

Kunz, M., Blahak, U., Handwerker, J., Schmidberger, M., Punge, H. J., Mohr, S., Fluck, E., and Bedka, K. M.: The severe hailstorm in southwest Germany on 28 July 2013: characteristics, impacts and meteorological conditions, Quarterly Journal of the Royal Meteorological Society, 144, 231–250, https://doi.org/10.1002/qj.3197, 2018.

Li, F., Chavas, D. R., Reed, K. A., and Dawson Ii, D. T.: Climatology of Severe Local Storm Environments and Synoptic-Scale Features over North America in ERA5 Reanalysis and CAM6 Simulation, Journal of Climate, 33, 8339–8365, https://doi.org/10.1175/JCLI-D-19-0986.1, 2020.

Lin, Y. and Kumjian, M. R.: Influences of CAPE on Hail Production in Simulated Supercell Storms, Journal of the Atmospheric Sciences, 79, 179–204, https://doi.org/10.1175/JAS-D-21-0054.1, 2022.

Lock, N. A. and Houston, A. L.: Empirical Examination of the Factors Regulating Thunderstorm Initiation, Monthly Weather Review, 142, 240–258, https://doi.org/10.1175/MWR-D-13-00082.1, 2014.

López, L., García-Ortega, E., and Sánchez, J. L.: A short-term forecast model for hail, Atmospheric Research, 83, 176–184, https://doi.org/10.1016/j.atmosres.2005.10.014, 2007.

Madonna, E., Ginsbourger, D., and Martius, O.: A Poisson regression approach to model monthly hail occurrence in Northern Switzerland using large-scale environmental variables, Atmospheric Research, 203, 261–274, https://doi.org/10.1016/j.atmosres.2017.11.024, 2018.

Mansfield, E. R. and Helms, B. P.: Detecting Multicollinearity, The American Statistician, 36, 158, https://doi.org/10.2307/2683167, 1982.

Manzato, A.: Hail in Northeast Italy: Climatology and Bivariate Analysis with the Sounding-Derived Indices, Journal of Applied Meteorology and Climatology, 51, 449–467, https://doi.org/10.1175/JAMC-D-10-05012.1, 2012.

Markowski, P. and Richardson, Y.: Mesoscale Meteorology in Midlatitudes, Wiley, 1 edn., https://doi.org/10.1002/9780470682104, 2010.

Martius, O., Kunz, M., Nisi, L., and Hering, A.: Conference Report 1st European Hail Workshop, Meteorologische Zeitschrift, 24, 441–442, https://doi.org/10.1127/metz/2015/0667, 2015.

Melcón, P., Merino, A., Sánchez, J. L., López, L., and García-Ortega, E.: Spatial patterns of thermodynamic conditions of hailstorms in southwestern France, Atmospheric Research, 189, 111–126, https://doi.org/10.1016/j.atmosres.2017.01.011, 2017.

Meteotest: Nationales Hagelprojekt. Schlussbericht: Aufbereitung historische Hagel-Daten, Tech. rep., Meteotest AG, Bern, access upon request., 2021.

Miller, R.: Notes on Analysis and Severe-storm Forecasting Procedures of the Air Force Global Weather Central, Tech. rep., Air Weather Service (MAC) United States Airforce, 1972.

https://doi.org/10.5194/egusphere-2024-371
Preprint. Discussion started: 23 February 2024

Mohr, S. and Kunz, M.: Recent trends and variabilities of convective parameters relevant for hail events in Germany and Europe, Atmospheric Research, 123, 211–228, https://doi.org/10.1016/j.atmosres.2012.05.016, 2013.

Mohr, S., Kunz, M., and Geyer, B.: Hail potential in Europe based on a regional climate model hindcast: HAIL POTENTIAL IN EUROPE, Geophysical Research Letters, 42, 10,904–10,912, https://doi.org/10.1002/2015GL067118, 2015a.

Mohr, S., Kunz, M., and Keuler, K.: Development and application of a logistic model to estimate the past and future hail potential in Germany: LOGISTIC MODEL ESTIMATING HAIL POTENTIAL, Journal of Geophysical Research: Atmospheres, 120, 3939–3956, https://doi.org/10.1002/2014JD022959, 2015b.

Moncrieff, M. W. and Miller, M. J.: The dynamics and simulation of tropical cumulonimbus and squall lines, Quarterly Journal of the Royal Meteorological Society, 102, 373–394, https://doi.org/10.1002/qj.49710243208, 1976.

Mulholland, J. P., Peters, J. M., and Morrison, H.: How Does LCL Height Influence Deep Convective Updraft Width?, Geophysical Research Letters, 48, e2021GL093 316, https://doi.org/10.1029/2021GL093316, 2021.

Nisi, L., Martius, O., Hering, A., Kunz, M., and Germann, U.: Spatial and temporal distribution of hailstorms in the Alpine region: a long-term, high resolution, radar-based analysis, Quarterly Journal of the Royal Meteorological Society, 142, 1590–1604, https://doi.org/10.1002/qj.2771, 2016.

Nisi, L., Hering, A., Germann, U., and Martius, O.: A 15-year hail streak climatology for the Alpine region, Quarterly Journal of the Royal Meteorological Society, 144, 1429–1449, https://doi.org/10.1002/qj.3286, 2018.

Nisi, L., Hering, A., Germann, U., Schroeer, K., Barras, H., Kunz, M., and Martius, O.: Hailstorms in the Alpine region: Diurnal cycle, characteristics, and the nowcasting potential of lightning properties, Quarterly Journal of the Royal Meteorological Society, 146, 4170–4194, https://doi.org/10.1002/qj.3897, 2020.

Nixon, C. J., Allen, J. T., and Taszarek, M.: Hodographs and Skew Ts of Hail-Producing Storms, Weather and Forecasting, 38, 2217–2236, https://doi.org/10.1175/WAF-D-23-0031.1, 2023.

Piasecki, K., Matczak, P., Taszarek, M., Czernecki, B., Skop, F., and Sobisiak, A.: Giant hail in Poland produced by a supercell merger in extreme instability – A sign of a warming climate?, Atmospheric Research, 292, 106 843, https://doi.org/10.1016/j.atmosres.2023.106843, 2023.

Pilguj, N., Taszarek, M., Allen, J. T., and Hoogewind, K. A.: Are Trends in Convective Parameters over the United States and Europe Consistent between Reanalyses and Observations?, Journal of Climate, 35, 3605–3626, https://doi.org/10.1175/JCLI-D-21-0135.1, 2022.

Piper, D. and Kunz, M.: Spatiotemporal variability of lightning activity in Europe and the relation to the North Atlantic Oscillation teleconnection pattern, Natural Hazards and Earth System Sciences, 17, 1319–1336, https://doi.org/10.5194/nhess-17-1319-2017, 2017.

Punge, H. and Kunz, M.: Hail observations and hailstorm characteristics in Europe: A review, Atmospheric Research, 176-177, 159–184, https://doi.org/10.1016/j.atmosres.2016.02.012, 2016.

Púčik, T., Groenemeijer, P., Rýva, D., and Kolář, M.: Proximity Soundings of Severe and Nonsevere Thunderstorms in Central Europe, Monthly Weather Review, 143, 4805–4821, https://doi.org/10.1175/MWR-D-15-0104.1, 2015.

Púčik, T., Castellano, C., Groenemeijer, P., Kühne, T., Rädler, A. T., Antonescu, B., and Faust, E.: Large Hail Incidence and Its Economic and Societal Impacts across Europe, Monthly Weather Review, 147, 3901–3916, https://doi.org/10.1175/MWR-D-19-0204.1, 2019.

Rasmussen, E. N.: Refined Supercell and Tornado Forecast Parameters, Weather and Forecasting, 18, 530–535, https://doi.org/10.1175/1520-0434(2003)18<530:RSATFP>2.0.CO;2, 2003.

Raupach, T. H., Soderholm, J., Protat, A., and Sherwood, S. C.: An Improved Instability–Shear Hail Proxy for Australia, Monthly Weather Review, 151, 545–567, https://doi.org/10.1175/MWR-D-22-0127.1, 2023a.

https://doi.org/10.5194/egusphere-2024-371
Preprint. Discussion started: 23 February 2024

Raupach, T. H., Soderholm, J. S., Warren, R. A., and Sherwood, S. C.: Changes in hail hazard across Australia: 1979–2021, npj Climate and Atmospheric Science, 6, 143, https://doi.org/10.1038/s41612-023-00454-8, 2023b.

Roebber, P. J.: Visualizing Multiple Measures of Forecast Quality, Weather and Forecasting, 24, 601–608, https://doi.org/10.1175/2008WAF2222159.1, 2009.

Rohrer, M., Brönnimann, S., Martius, O., Raible, C. C., and Wild, M.: Decadal variations of blocking and storm tracks in centennial reanalyses, Tellus A: Dynamic Meteorology and Oceanography, 71, 1586 236, https://doi.org/10.1080/16000870.2019.1586236, 2019.

Rädler, A. T., Groenemeijer, P., Faust, E., and Sausen, R.: Detecting Severe Weather Trends Using an Additive Regressive Convective Hazard Model (AR-CHaMo), Journal of Applied Meteorology and Climatology, 57, 569–587, https://doi.org/10.1175/JAMC-D-17-0132.1, 2018.

Rädler, A. T., Groenemeijer, P. H., Faust, E., Sausen, R., and Púčik, T.: Frequency of severe thunderstorms across Europe expected to increase in the 21st century due to rising instability, npj Climate and Atmospheric Science, 2, 30, https://doi.org/10.1038/s41612-019-0083-7, 2019.

Schemm, S., Nisi, L., Martinov, A., Leuenberger, D., and Martius, O.: On the link between cold fronts and hail in Switzerland: On the link between cold fronts and hail in Switzerland, Atmospheric Science Letters, 17, 315–325, https://doi.org/10.1002/asl.660, 2016.

Schmeits, M. J., Kok, K. J., and Vogelezang, D. H. P.: Probabilistic Forecasting of (Severe) Thunderstorms in the Netherlands Using Model Output Statistics, Weather and Forecasting, 20, 134–148, https://doi.org/10.1175/WAF840.1, 2005.

Schmid, T., Portmann, R., Villiger, L., Schröer, K., and Bresch, D. N.: An open-source radar-based hail damage model for buildings and cars, preprint, Atmospheric, Meteorological and Climatological Hazards, https://doi.org/10.5194/nhess-2023-158, 2023.

Schröer, K., Trefalt, S., Hering, A., Germann, U., and Schwierz, C.: Hagelklima Schweiz: Daten, Ergebnisse und Dokumentation: Fachbericht MeteoSchweiz No. 283, Tech. rep., MeteoSchweiz, https://doi.org/10.18751/PMCH/TR/283.HAGELKLIMASCHWEIZ/1.0, 2023.

Schwarz, G.: Estimating the Dimension of a Model, Annals of Statistics, 6, 461–464, https://ui.adsabs.harvard.edu/abs/1978AnSta...6..461S, aDS Bibcode: 1978AnSta...6..461S, 1978.

Showalter, A. K.: A Stability Index for Thunderstorm Forecasting, Bulletin of the American Meteorological Society, 34, 250–252, https://doi.org/10.1175/1520-0477-34.6.250, 1953.

Sánchez, J. L., Marcos, J. L., Dessens, J., López, L., Bustos, C., and García-Ortega, E.: Assessing sounding-derived parameters as storm predictors in different latitudes, Atmospheric Research, 93, 446–456, https://doi.org/10.1016/j.atmosres.2008.11.006, 2009.

Taszarek, M., Allen, J. T., Púčik, T., Hoogewind, K. A., and Brooks, H. E.: Severe Convective Storms across Europe and the United States. Part II: ERA5 Environments Associated with Lightning, Large Hail, Severe Wind, and Tornadoes, Journal of Climate, 33, 10 263–10 286, https://doi.org/10.1175/JCLI-D-20-0346.1, 2020a.

Taszarek, M., Pilguj, N., Allen, J. T., Gensini, V., Brooks, H. E., and Szuster, P.: Comparison of convective parameters derived from ERA5 and MERRA2 with rawinsonde data over Europe and North America, Journal of Climate, pp. 1–55, https://doi.org/10.1175/JCLI-D-20-0484.1, 2020b.

Taszarek, M., Allen, J. T., Brooks, H. E., Pilguj, N., and Czernecki, B.: Differing Trends in United States and European Severe Thunderstorm Environments in a Warming Climate, Bulletin of the American Meteorological Society, 102, E296–E322, https://doi.org/10.1175/BAMS-D-20-0004.1, 2021.

Taylor, C. M.: Detecting soil moisture impacts on convective initiation in Europe, Geophysical Research Letters, 42, 4631–4638, https://doi.org/10.1002/2015GL064030, 2015.

Tippett, M. K., Allen, J. T., Gensini, V. A., and Brooks, H. E.: Climate and Hazardous Convective Weather, Current Climate Change Reports, 1, 60–73, https://doi.org/10.1007/s40641-015-0006-6, 2015.

https://doi.org/10.5194/egusphere-2024-371
Preprint. Discussion started: 23 February 2024

Trefalt, S.: Hail and Severe Wind Gusts in the Convective Season in Switzerland, Ph.D. thesis, Philosophisch-naturwissenschatliche Fakultät der Universität Bern, 2017.

Trefalt, S., Germann, U., Hering, A., Clementi, L., Boscacci, M., Schröer, K., and Schwierz, C.: Hail Climate Switzerland Operational radar hail detection algorithms at MeteoSwiss: quality assesssment and improvement: Fachbericht MeteoSchweiz No. 284, Tech. rep., MeteoSchweiz, https://doi.org/10.18751/PMCH/TR/284.HAILCLIMATESWITZERLAND/1.0, 2023.

Tuovinen, J.-P., Rauhala, J., and Schultz, D. M.: Significant-Hail-Producing Storms in Finland: Convective-Storm Environment and Mode, Weather and Forecasting, 30, 1064–1076, https://doi.org/10.1175/WAF-D-14-00159.1, 2015.

Varga, A. J. and Breuer, H.: Evaluation of convective parameters derived from pressure level and native ERA5 data and different resolution WRF climate simulations over Central Europe, Climate Dynamics, 58, 1569–1585, https://doi.org/10.1007/s00382-021-05979-3, 2022.

Waldvogel, A., Federer, B., and Grimm, P.: Criteria for the Detection of Hail Cells, Journal of Applied Meteorology, 18, 1521–1525, https://doi.org/10.1175/1520-0450(1979)018<1521:CFTDOH>2.0.CO;2, 1979.

Weisman, M. L. and Klemp, J. B.: The Dependence of Numerically Simulated Convective Storms on Vertical Wind Shear and Buoyancy, Monthly Weather Review, 110, 504–520, https://doi.org/10.1175/1520-0493(1982)110<0504:TDONSC>2.0.CO;2, 1982.

Weisman, M. L. and Klemp, J. B.: The Structure and Classification of Numerically Simulated Convective Stormsin Directionally Varying Wind Shears, Monthly Weather Review, 112, 2479–2498, https://doi.org/10.1175/1520-0493(1984)112<2479:TSACON>2.0.CO;2, 1984.

Wiese, W.: Polareis Und Atmosphärische Schwankungen, Geografiska Annaler, 6, 273–299, https://doi.org/10.1080/20014422.1924.11881099, 1924.

Willemse, S.: A statistical analysis and climatological interpretation of hailstorms in Switzerland, Ph.D. thesis, ETH Zurich, https://doi.org/10.3929/ETHZ-A-001486581, medium: application/pdf,X, 176, 13 S., 1995.

Wu, J., Guo, J., Yun, Y., Yang, R., Guo, X., Meng, D., Sun, Y., Zhang, Z., Xu, H., and Chen, T.: Can ERA5 reanalysis data characterize the pre-storm environment?, Atmospheric Research, 297, 107 108, https://doi.org/10.1016/j.atmosres.2023.107108, 2024.